

Highlights:

- An obstacle-related drift is created along an uplifted ridge and mud volcano
- drift-architecture and bottom current strength differ from the Cadiz-CDS
- Mud extrusions interfere with bottom currents and sedimentation patterns
- CWC mounds are present, incorporated within the sedimentary sequence

1 Stratigraphy and palaeoceanography of a topography-controlled
2 contourite drift in the Pen Duick area, southern Gulf of Cadiz

3 Vandorpe T.¹, Van Rooij, D.¹, de Haas, H.²

4 ¹Ghent University, Department of Geology & Soil Science, Renard Centre of Marine Geology,
5 Krijgslaan 281 S8, 9000 Ghent, Belgium

6 ²NIOZ Royal Netherlands Institute for Sea Research, Department of Marine Geology, P.O.
7 Box 59, 1790 AB Den Burg, The Netherlands

8

9

10

11

12 Corresponding author:

13 Vandorpe Thomas

14 Krijgslaan 281, S8

15 9000 Gent

16 Belgium

17 Email: Thomas.vandorpe@ugent.be

18

19 **Abstract**

20 The northern part of the Gulf of Cadiz has and still is receiving a lot of attention from the scientific
21 community due to (amongst others) the recent IODP Expedition 339. On the contrary, the southern
22 part of the Gulf received far less attention, although mud volcanoes, diapiric ridges and cold-water
23 corals are present in this region. The El Arraiche mud volcano field is characterized by a compressive
24 regime (opposed to the extensive regime in most of the Gulf), creating several ridges and aiding the
25 migration of hydrocarbons towards the surface. This study presents seismic and multibeam evidence
26 for the existence of a contourite drift along the southwestern flanks of the Pen Duick escarpment
27 (PDE) and Gemini mud volcano, within the El Arraiche mud volcano field. From the start of the
28 Quaternary, when the escarpment started to lift and the mud volcano originated, contouritic
29 deposition was initiated at the foot of both topographies. Initially, fairly low-speed bottom currents
30 gave rise to sheeted drift deposits, affected by the uplift of the PDE or extrusion of mud. From the
31 Mid-Pleistocene onwards, separated mounded drift deposits formed due to intensified bottom
32 currents. An AAIW origin for the drift is proposed based on CTD data, whereas the influence of the
33 Mediterranean Outflow Water (MOW) is not observed. Moreover, the changes recorded within this
34 contourite drift differ from the MOW-dominated contourite depositional system in the northern Gulf
35 of Cadiz, as drift deposits only occur as early as the base of the Quaternary (compared to the Early-
36 Pliocene for the north) and mounded drift deposits only occur from the Middle-Pleistocene onwards
37 (compared to the Early-Pleistocene). Cold-water coral mounds have been found within and on top of
38 the sedimentary sequence at the foot of the PDE. This implies that environmental conditions in which
39 cold-water corals thrive were present in the past at the foot of the PDE and not only on top.

40 **Keywords:** Gulf of Cadiz, Contourite drift, Pen Duick escarpment, mud volcano, seismic stratigraphy,
41 Antarctic Intermediate Water

42 **Highlights:**

- 43
- An obstacle-related drift is created along an uplifted ridge and mud volcano

- 44 • drift-architecture and bottom current strength differ from the Cadiz-CDS
- 45 • Mud extrusions interfere with bottom currents and sedimentation patterns
- 46 • CWC mounds are present, incorporated within the sedimentary sequence

47

48 **1. Introduction**

49 Contourite deposits have first been recognized in the 1960's (Heezen et al., 1966) and were initially
50 exclusively associated to thermohaline currents. Especially the deposits along the eastern North
51 American margin, shaped by the western boundary undercurrent, have been studied (Locker and
52 Laine, 1992; Mccave and Tucholke, 1986; Schneider et al., 1967). From then onwards, gradually a
53 larger variety of contourite expressions, both in small or large scale, have been discovered (Duarte
54 and Viana, 2007; Faugères and Stow, 1993a; Faugères and Stow, 1993b; Hernández-Molina et al.,
55 2011). Other factors, as obstacles and internal waves, are now also acknowledged for being able to
56 create contourite deposits (Hernández-Molina et al., 2006a; Preu et al., 2013; Rebesco et al.,
57 submitted). As a consequence, the definition of contourites has been adapted to sediments
58 deposited or significantly affected by bottom currents (Rebesco et al., 2005; Stow et al., 2002). Not
59 only depositional, but erosional features (furrows, moats, scours, ...) are generated as well by bottom
60 currents (Hernández-Molina et al., 2006b). Due to their enhanced sedimentation rates, contourites
61 are ideal recorders for palaeoclimatological and palaeoceanographic information, since they are
62 influenced by bottom currents and their association with climate is well established (Cacho et al.,
63 2000; Frigola et al., 2008; Llave et al., 2007). Due to the important role of bottom current in sorting
64 grain size classes, the economic potential of these deposits as reservoir systems may not be
65 underestimated (Antich et al., 2005; Llave et al., 2005; Rebesco et al., submitted; Viana et al., 2007).
66 Besides their ability to deposit laterally continuous muddy contourite sheets, operating as an
67 impermeable seal, long-lasting bottom currents may also create extensive and "clean" sand sheets;
68 e.g. the Campos basin sands, Brazil (Viana et al., 1998a) or the Grand Bank sands, NW Atlantic,

69 offshore Newfoundland (Dalrymple et al., 1992). These could serve as reservoirs (Viana et al., 2007;
70 Viana et al., 1998b).

71 In the Gulf of Cadiz (GoC), a large contourite depositional system (CDS) is present along the Iberian
72 margin due to the Mediterranean Outflow Water (MOW) (García et al., 2009; Hernández-Molina et
73 al., 2006b; Llave et al., 2001; Llave et al., 2006; Stow and Hernández-Molina, 2006). A CDS is the
74 association of various drifts and related erosional features and may vary laterally as well as vertically
75 (Hernández-Molina et al., 2008). The GoC CDS has been studied extensively over the past decades as
76 it very large (over 10000 km²), recorded the major changes of the MOW and has an important sand
77 content (Hans Nelson et al., 1993; Hernández-Molina et al., 2006b; Roque et al., 2012; Toucanne et
78 al., 2007). The global interest in this system resulted in IODP Expedition 339 (November 2011-
79 January 2012). This campaign aimed at studying in detail the climatic and oceanographic changes in
80 the Cadiz area and the effect this had on a global scale as well as the distribution of clean and well
81 sorted sand deposits (Expedition 339 scientists, 2012). In contrast to the enormous attention for the
82 northern part, the southern GoC remained largely unstudied up till recently, although a southern
83 branch of the MOW is reported and meddies (Mediterranean eddies) are found in the southern Gulf
84 of Cadiz (Ambar et al., 2008; Richardson et al., 2000).

85 The El Arraiche mud volcano field has been studied extensively in the last decade because of several
86 factors. First, an extensional tectonic regime within a compressional area is present (Flinch, 1993).
87 This results in the presence of extensional ridges (of which the Pen Duick escarpment is one, see Fig.
88 2), characterized by rotated blocks and bound by lystric faults (Van Rensbergen et al., 2005).
89 Secondly, many mud volcanoes (MV, e.g. Gemini MV, see Fig. 2) have been recognized and
90 investigated in the region (Perez-Garcia et al., 2011; Van Rensbergen et al., 2005) and are thought to
91 be the results of subsurface diapirism (Haffert et al., 2013; Perez-Garcia et al., 2011). Mud volcano
92 activity is estimated to have started 2.4 Ma ago (Van Rensbergen et al., 2005) and happened in
93 several phases (Perez-Garcia et al., 2011). Thirdly, the discovery of cold-water corals (CWC) in the

94 GoC triggered a lot of research (Foubert et al., 2008; Van Rooij et al., 2011; Wienberg et al., 2010).
95 Only a few living CWC are found in the area (De Mol et al., 2011), mostly fossil corals or coral rubble
96 is found (Wienberg et al., 2010; Wienberg et al., 2009). This can be attributed to changing
97 environmental conditions (palaeo-productivity, palaeoceanography and change in food supply) which
98 were more favourable during glacial periods in the GoC (Van Rooij et al., 2011; Wienberg et al.,
99 2010). Along the northern east-Atlantic margins (Porcupine, Norway), CWC are thriving nowadays
100 (Frank et al., 2009). Past environmental conditions are difficult to assess as many of the mounds
101 show signs of early diagenesis and are subject to erosion once growth is absent (Foubert et al., 2008;
102 Frank et al., 2009; Templer et al., 2011; Wehrmann et al., 2011). As a consequence, the palaeo-
103 environmental conditions have to be inferred from different parameters. The off-mound history,
104 recorded within drift deposits, may be a good possibility for this.

105 A small-scale contourite drift is known from the foot of the Pen Duick Escarpment (Fig. 2) (Van Rooij
106 et al., 2011), proposed here to be named the Pen Duick escarpment drift. The position at the foot of
107 the Pen Duick escarpment (Fig. 2) and its location at the foot of several corals mounds make sure this
108 drift is of great interest to the scientific community. This paper attempts to unravel the spatial and
109 temporal evolution of the Pen Duick drift, the involved oceanographic processes and in which way
110 the evolution of the contourite drift was influenced by periods of mud activity. In relation, does the
111 contourite drift contain information on the palaeoceanographic variability of the region and its
112 influence on CWC mound growth?

113 **2. Regional setting**

114 **2.1. Geology & geomorphology**

115 The present-day structure and geomorphology of the Gulf of Cadiz is the result of several episodes of
116 rifting, extension and compression from the Triassic onwards (Maldonado et al., 1999; Medialdea et
117 al., 2004). Large allochthonous wedges have been emplaced due to ongoing oblique European-African
118 convergence and the westward motion of the Gibraltar Arc (Middle Miocene), creating the Alboran

119 domain (Maldonado et al., 1999). The sedimentary cover on top of this allochthonous wedge is
120 Neogene in age and is pierced by numerous mud volcanoes (Medialdea et al., 2009; Somoza et al.,
121 2003), salt diapirs (Lolita salt diaper), diapiric ridges (Donana and Cadiz diapiric ridge) and fluid
122 escape features, such as pockmarks (Fig. 1). Most mud volcanoes lie within the offshore Betic-Rifian
123 domain of the accretionary wedge (Medialdea et al., 2004) and are grouped into several fields: the
124 Guadalquivir ridge field, the TAYSO field, the deep Portuguese margin field and the Spanish-
125 Moroccan margin field (Fig. 1). The migration of hydrocarbon fluids towards the surface is facilitated
126 by the presence of many faults and they in turn fuel the mud volcanoes (Pinheiro et al., 2003; Tingay
127 et al., 2003; Van Rensbergen et al., 2005).

128 The Pen Duick Escarpment (PDE) is situated in the southern Gulf of Cadiz, between 35°10'N to
129 35°30'N and 6°30'W to 6°55'W (Figs. 1, 2). It is a part of the Renard Ridge that originated due to the
130 compressive regime in the area, which is in contrast to the extensional regime in the main part of the
131 Gulf of Cadiz (Van Rensbergen et al., 2005). The ridges are bounded by lystric faults (Flinch, 1993)
132 and the compression is estimated to have started 2.4 Ma ago (Van Rensbergen et al., 2005), coeval
133 with the Upper Pliocene Revolution, which marks the onset of the northern hemisphere glaciations
134 and the present-day oceanic circulation (Haq et al., 1987; Hernández-Molina et al., 2002; Lowrie,
135 1986; Maldonado et al., 1999). Seven mud volcanoes are observed in this area, known as the El
136 Arraiche Mud Volcanoe province (Van Rensbergen et al., 2005) and they are part of the Spanish-
137 Moroccan margin field (Fig. 1).

138 CWCs mounds occur on top of Renard Ridge (of which the PDE is a part) (Foubert et al., 2008;
139 Wehrmann et al., 2011) and they form juvenile mounds, like Alpha, Beta and Gamma mound (De Mol
140 et al., 2011; Foubert et al., 2008; Frank et al., 2009). Their occurrence on top of the ridge is the result
141 of both hydrodynamic (currents) and geological (seepage) factors. A three-stage model for CWC
142 mound growth has been proposed by Foubert et al. (2008). First of all, oceanographic, environmental
143 and food-supply conditions need to be right. Wienberg et al. (2010) proved that mound growth

144 prevailed during glacial periods due to enhanced productivity conditions (more Aeolian dust and
145 increased upwelling). Secondly, sedimentation (or the absence of it) becomes important for the
146 mound growth. The supply of food particles and prevention of burial occurs due to increased bottom
147 currents (Van Rooij et al., 2011; Wienberg et al., 2010; Wienberg et al., 2009). Thirdly, diagenetic
148 processes (aragonite dissolution and carbonate precipitation) become important throughout the
149 mound growth (Pirlet et al., 2010). Wehrmann et al. (2011) proved the affection of mounds by
150 ascending methane-bearing fluids, inducing diagenetic processes.

151 Accumulation rates for mound growth as high as 220 cm/ka have been reported during glacials, while
152 during times of reduced mound development (mostly interglacials), only growth rates of 0 to 5 cm/ka
153 have been reported (Frank et al., 2009).

154 **2.2. Oceanography**

155 The oceanography of the northern Gulf of Cadiz is well known due to the presence of the extensively
156 studied contourite depositional system (CDS) originating from the Mediterranean Outflow Water
157 (MOW) (Hernández-Molina et al., 2006b; Llave et al., 2006; Millot, 2009; Stow and Hernández-
158 Molina, 2006). This warm and saline water mass flows out of the Mediterranean Sea via the Gibraltar
159 Strait and continues as an intermediate water mass (500 to 1400 meters water depth) along the
160 Southern Iberian slope due to Coriolis deflection. After its exit out of the Strait of Gibraltar, the MOW
161 is split up into two main branches: the upper and lower Mediterranean waters (García, 2002;
162 Hernández-Molina et al., 2006b). The upper core flows along the shelf edge at depths of 500 to 800
163 meters and the lower core at depths of 750 to 1400 meters to the west-northwest. This last branch
164 splits up into three major branches (from north to south): the intermediate, the principal and the
165 southern branch (Fig. 1) (Louarn and Morin, 2011).

166 On the contrary, the oceanography of the southern Gulf of Cadiz is less studied. In the PDE area (area
167 shown in Fig. 2), 4 water masses are known to occur: the North Atlantic Surface Water (NASW, 0-100
168 m), the North Atlantic Central Water (NACW, 100-600 m), the Antarctic Intermediate Water (AAIW,

169 600-1500 m) and the North Atlantic Deep Water (NADW, beneath 1500 m) (Ambar et al., 2008;
170 Louarn and Morin, 2011; Machín et al., 2006a). NASW represents the upper 100 meters of the water
171 column and consists of modified NACW. NACW is characterized by a linear decrease in temperature
172 (16°-12°C) and salinity (36.25-35.5) (Criado-Aldeanueva et al., 2006; Louarn and Morin, 2011) and
173 flows from west to east in the Gulf of Cadiz. NACW splits up in the Gulf of Cadiz: it recirculates
174 southwards along the African coast due to deflection of a coastal upwelling zone, northwards along
175 the Iberian margin and another branch flows directly into the Mediterranean Sea (Fig. 1) (Machín et
176 al., 2006b). The general circulation pattern of these upper two water masses is anticyclonic, as
177 they are part of the Azores current, which is in turn part of the northeastern Atlantic circulation
178 (Machín et al., 2006a). AAIW is characterized by low oxygen and high silicate values. Although
179 intensive mixing with under- and overlying water masses makes its direct recognition problematic,
180 AAIW is known to flow northwards along the African coast in the southern Gulf of Cadiz, before being
181 outcompeted in the north by MOW. Salinity values of AAIW (35.6) are slightly higher than the values
182 of the lower NACW (35.45) (Louarn and Morin, 2011). NADW is present below 1500 meters and flows
183 from south to north in the Gulf of Cadiz (Fig. 1), along the Atlantic margin. It is characterized by low
184 salinities (<35.5) and temperatures (<8°C) (Louarn and Morin, 2011).

185 The PDE experiences the influence of NACW at its top (550 meters water depth) and AAIW at its foot
186 (650 meters water depth, Fig. 3) (Van Rooij et al., 2011). At present, MOW does not occur along the
187 PDE, as Mediterranean waters are not observed above 700 meters water depth (Fig. 3) (Mienis et al.,
188 2012) and CTD data do not indicate their presence (Van Rooij et al., 2011) (Fig. 3). However, meddies
189 are known to transport MOW south of the Strait of Gibraltar (Fig. 3) (Ambar et al., 2008; Richardson
190 et al., 2000) and the MOW is strongly influenced by glacial-interglacial alternations, with a stronger
191 MOW during glacial periods (Toucanne et al., 2007). So, the influence of the MOW in the region
192 cannot be excluded, certainly as Van Rooij et al. (2011) and Foubert et al. (2008) inferred the
193 possibility of an intensified glacial MOW, being able to reach the PDE through enhanced meddy
194 activity.

195 **3. Material and methods**

196 Within the framework of the R/ V Belgica “CADIPOR” cruises (2001, 2005 and 2007) and the “Pen
197 Duick” campaign (2009) in the southern GoC, a total of 520 km high-resolution single channel seismic
198 sparker profiles have been acquired at the foot of the Pen Duick escarpment and the Gemini mud
199 volcano. A SIG sparker (80 electrodes in 2001, 120 electrodes in 2005, 2007 and 2009) has been used,
200 with a shot interval of 2 seconds (3 seconds in 2009). The energies reached 500 J and a 8 kHz
201 sampling frequency has been used. A record length of 1.6 s TWT (in 2001), 1.8 s TWT (in 2005 and
202 2007) and 2.5 s TWT (in 2009) was obtained. The profiles were acquired with acquisition velocities
203 within the range of 3 to 4 knots.

204 The profiles (Figs. 5, 6 and 7) have been processed using the DECO Geophysical RadexPro processing
205 software. A swell filter, bandpass filter (Butterworth type, low cut at 200 Hz, low-cut slope of 24 dB/s
206 and high cut at 1500 Hz, high-cut slope of 36 dB/s), predictive deconvolution, 2D spike removal and
207 amplitude corrections have been applied.

208 The multibeam data (in total 700 km²), recorded during the CADIPOR I cruise (2001) have been
209 obtained using the SIMRAD EM1002 system, extended with a deep water module, permanently
210 installed on R/V Belgica. The swath width was 500 meter above 500 meters water depth and 750
211 meters below. The data have been corrected and cleaned using Kongsberg’s Merlin and Neptune
212 packages. The footprint at 400 meters water depth is 15x15 meters. This dataset was already
213 extensively described with respect to the main geomorphological features and mud volcanoes within
214 Van Rensbergen et al. (2005).

215 Profile M2005_105 (Fig. 4) has been acquired by the R/V Pelagia in 2006 within the framework of the
216 ESF EuroDIVERSITY MiCROSYSTEMS project. Three airguns (10, 20 and 40 cubic inch volume) were
217 used and they were towed in a frame at 1.3, 1.8 and 2.0 meters depth. The guns were towed 37
218 meters behind the stern of the ship and fired every 5 seconds at a pressure of 100 bars, resulting in
219 an average distance between the shots of 10.5 meters (4.2 knots sailing speed). The streamer (towed

220 at a depth of 1 meter below surface) consists of four 63 meter long sections with 6 channels each.
221 Each channel has 10 Teledyne T2 hydrophones (interval of 1 m). The data were recorded by the Geo-
222 Resources Geo-Trace 24 hard- and software system, consisting of a 24 channel digital pre-
223 amplification system. The record length was 2000 ms TWT and the sampling interval 0.5 ms. When
224 recording, a bandpass filter (30 Hz high pass and 700 low pass) was applied. On board, the lines were
225 stacked and preliminary migration has been performed.

226 **4. Results**

227 **4.1 Geomorphology**

228 The study area extends from 35° 22' N to 35° 14' N and 6° 52' W to 6° 45' W (Fig. 2). Within the
229 investigated area, the multibeam data show the presence of the PDE (about 80-100 meters above
230 the seafloor), three mud volcanoes (e.g. Gemini MV, about 150 meters high), CWC mounds (on top of
231 the PDE, previously discussed by amongst others De Mol et al. (2011) and Templer et al. (2011)) and
232 6 mounded structures along the foot of the PDE. They have a diameter between 200 and 300 meters
233 and are between 5 and 10 meters high.

234 A semi-continuous channel, with widths varying between 200 and 300 meters, is present along the
235 foot of the aforementioned topographies (Fig. 2). The channel is about 10 km long from its most
236 southeastern (along Gemini mud volcano) till its most northwestern (northern boundary PDE)
237 expression. The first 2 km of this channel have an east-west direction, following the southern border
238 of the Gemini MV. Here, the most pronounced expression of the channel is observed with depths
239 differences up to 15 m (see inset Fig. 2). Then, it changes to a south-southeast to north-northwest
240 direction for 8 km, following the base of the Gemini MV and PDE, respectively. When the channel
241 passes the boundary between the Gemini MV and the PDE, the depth decreases strongly (to about 5
242 m) and increases again along the PDE. Along the PDE, the depth of the channel varies between 5 and
243 15 m, with a gradual decrease in expression towards the first of the six mounds. Along these mounds,
244 two channels are observed: one which continues along the foot of the PDE and increases in depth, to

245 former values of about 15 m and a second one WSW of the mounds (depths of about 15 m). Both
246 gradually lose their expression to the northwest.

247 Immediately south (along the Gemini MV) or southwest (along the PDE) of the channel, mounded
248 sediments are present. They rise about 3 to 5 m above the smoothly dipping (about 1° SW) seafloor
249 south (-west) of them and 5 to 20 m above the base of the channel (see inset Fig. 2).

250 **4.2 Seismic stratigraphy**

251 Based on the seismic sparker profiles and the multichannel airgun profile, 5 seismic stratigraphic
252 units have been discerned, separated by 4 discontinuities D1 to D4. Due to the lower penetration of
253 the sparker source (about 400 ms TWT, while at least 800 ms TWT for the airgun), only 4 of the 5
254 units are visible on the high-frequency sparker profiles. The PDE and Gemini MV can be considered as
255 the acoustic basement in the ENE, but in the WSW, no real acoustic basement is observed. This due
256 to attenuation of the signal in the thick sedimentary package. Reflectors can be distinguished in the
257 sparker profiles up to depths of about 1200 ms TWT (Figs. 5,6,7) and down to 1700 ms TWT in the
258 airgun profile (Fig. 4). Below this depth, the multiple inhibits its further recognition. Fig. 4 shows that
259 (semi-) continuous deposits of units 1 to 5 are bounded by the PDE or Gemini MV in the northeast
260 and a palaeohigh in the southwest. In the southwest, the palaeohigh rises to 150 to 200 ms beneath
261 the seafloor (Fig. 4). The seismic facies of the palaeohigh consists of very chaotic, discontinuous
262 reflectors of varying intensity. This facies differs from the seismic facies within the mud volcanoes in
263 the fact that the palaeohigh still contains reflections, while the mud volcanoes and tectonic ridges
264 have an almost acoustically transparent facies (Fig. 5, 6 and 7).

265 4.2.1 Unit 1

266 Unit 1 (only visible on Fig. 4) consists of low-amplitude semi-continuous reflectors at the base and
267 more continuous, slighter higher amplitude reflectors at the top. In the southwest, the unit is
268 intersected with many normal faults (see below). Unit 1 displays a more low-angle onlap onto the

269 basement in the east, while in the west a higher angle of onlap onto the palaeohigh is encountered
270 (Fig. 4). In Fig. 4, the top of the unit is incised deeply (± 60 ms TWT) along the Gemini MV.
271 Thicknesses of unit 1 vary between 150 ms TWT in the west-southwest and up to 550 ms TWT in the
272 middle of the basin. The maximum thickness cannot be calculated, as the multiple inhibits the
273 observation of the lower boundary (Fig. 4).

274 Unit 1 and a small part of unit 2 are affected by 2 distinct fault patterns: one major fault is located in
275 the centre of the basin and at least nine smaller ones to the west-southwest (Fig. 4). The large fault
276 (about 750 meters long and a dip of about 50-55°) is a normal, east-up fault with offsets of 10 ms
277 TWT at its top (about 1250 ms TWT), going to zero offsets at 1450 ms TWT. Deeper down, the offset
278 cannot be determined anymore due to a chaotic seismic expression. The smaller faults are normal,
279 east-up faults as well and all have offsets inferior to 5 ms TWT. Activity along the faults stop within
280 the lower part of Unit 2.

281 4.2.2. Unit 2

282 The boundary between units 1 and 2 is erosive, evidenced by the incision into unit 1 along the
283 Gemini MV (Fig. 4). Unit 2 consists of low to medium-amplitude, continuous reflectors at the base
284 and medium-amplitude, continuous reflectors at the top (Figs 5, 6). Overall, slightly mounded
285 deposits are present in this unit, observable about 500 meters SSW of the PDE and Gemini MV (Figs.
286 5, 6). Unit 2 fills a small incision at the intersection along the Gemini MV, showing a gradual decline
287 in incision upwards (only visible on Fig. 4). The base of the incision contains discontinuous, slightly
288 chaotic deposits, while more continuous deposits arise on top. Eight small cyclic subunits, each one
289 about 25 to 35 ms TWT thick (Figs. 5, 6) are observed within this unit. Subunit c has slightly higher
290 amplitude deposits, compared to the other 7 subunits. All subunits display very high amplitude
291 reflectors at their base and lower amplitudes on top. Along the PDE, the subunits are conform and
292 pinch-out of the reflectors is observed (Fig. 6), evidenced by the rise of individual reflectors (a
293 concave appearance) and a decrease in thickness of the subunits towards the PDE. The pinch-out is

294 greatest at the base of unit 2 and gradually diminishes upwards, nearly being absent at the top of
295 unit 2. Along the Gemini MV, a different pattern is observed: the subunits display small erosional
296 features. At the base of unit 2, first evidence of a Christmas-tree structure appears (Fig. 5). This
297 pattern of mud extrusions disrupts the sedimentation at the foot of the Gemini MV and can be
298 observed in all other units as well. The reflectors on top of these extrusions display a convex pattern
299 and gradually even out the extrusions (Fig. 5). Unit 2 is still faulted at its base, but the small
300 depression, left by the large fault, is gradually being evened out in this unit (Figs 4, 6). Thicknesses
301 vary between 200 and 250 ms TWT for most of the unit with a gradual decrease towards the
302 northwest (Fig. 8). In the west-southwest, thicknesses are reduced due to the presence of the
303 palaeohigh (Figs. 4, 8).

304 4.2.3. Unit 3

305 Units 2 and 3 are separated by an angular unconformity. Small-scale erosion has occurred along both
306 PDE and Gemini MV and the accommodation space is filled up by deposits of Unit 3 (Figs. 5, 6). Unit 3
307 has low-amplitude reflectors at its base and moderate-amplitude ones at its top along most of the
308 PDE (Fig. 6) and consists of mostly high-amplitude reflectors with a low-amplitude part in the middle
309 along the Gemini MV (Fig. 5). Four subunits have been discerned in this unit. The difference in
310 amplitudes of the different subunits is low (although some high-amplitude reflectors are present)
311 and they are distinguishable based on small angular unconformities (visible along both topographies,
312 Figs. 5, 6). A channel is present along the Gemini MV and a large part of the PDE with mounded
313 sediments on its south-western side. The channel is about 150 meters wide and incisions increase
314 upwards (5 ms TWT to 20 ms TWT). More erosion occurred along the PDE, as incisions are deeper
315 (Figs 5, 6).

316 Along the most northern part of the PDE, the unit has a different appearance: very high amplitudes
317 at the base, moderate in the middle and high again at the top (Fig. 7). Also, no evidence for a channel
318 along the PDE is observed here: the sedimentation pattern is obscured due to the presence of one of

319 the mounds and the resulting diffraction hyperbola. But what really sets it apart in this area is the
320 occurrence of 3 big and 2 small mounded structures within this unit (Fig. 7). They have an acoustically
321 almost transparent appearance. The two small ones (a few ms TWT high and less than 20 meters
322 wide) are situated deeper compared to the big ones (Fig. 7). The three big mounded structures
323 (between 20 and 30 ms TWT high and between 100 and 250 meters wide) originate at the same
324 stratigraphic level, depending on the position of the mound 15 to 25 ms TWT above the base of Unit
325 3 (Fig. 7). The sediments deposited on top display a concave appearance because of their presence.
326 Thicknesses are fairly constant and vary around 100 ms TWT, only along the mounds, 70 ms TWT of
327 sediment is present (Fig. 8). Slightly reduced values when approaching the PDE or Gemini MV (a
328 decrease of about 20 ms TWT) are observed as well (Fig. 8).

329 4.2.4 Unit 4

330 The boundary between units 3 and 4 (D3) is the most erosive one of the entire sedimentary
331 sequence. Along the PDE and Gemini MV, up to 25 ms TWT of sediments of Unit 3 are eroded by the
332 discontinuity, creating a channel with the same incision depth. The channel, which is present
333 throughout the entire unit, is filled differently along the PDE and Gemini MV (Figs. 5, 6). Along the
334 Gemini MV, continuous high-amplitude reflectors are encountered within the channel. They all have
335 a concave appearance (moat and mounded sediments) due to the continuing presence of a channel
336 (Fig. 5). Along the PDE, a heart-shaped block of chaotic and nearly reflection-free deposits is
337 encountered within the channel. This block has a small run-out and is up to 50 ms TWT thick and 300
338 meters long. Fig. 8 shows the position of these deposits. In the rest of the unit, high-amplitude,
339 nearly horizontal, continuous deposits are present (Figs. 5, 6).

340 Based on small erosional surfaces and changes in acoustic appearance, 3 subunits have been
341 discerned within Unit 4. The lowermost subunit (15-20 ms TWT thick) contains lower amplitudes
342 compared to the upper two (Figs. 5, 6). Within the upper subunit, along the PDE, a channel (about
343 100 meters wide and only a few ms TWT deep) is observed about 750 meters southwest of the PDE

344 (Fig. 6). Due to the thinning of this unit towards the north (Fig. 8), the subunits were no longer
345 discernable in Fig. 7. Unit 4 is the thinnest of the sedimentary sequence with values varying around
346 50 ms TWT (Fig. 8). At the position of the heart-shaped block, thicknesses go to zero.

347 4.2.5. Unit 5

348 A partly erosive boundary separates Units 4 and 5, although it is less erosive compared to the
349 previous discontinuity. Along the Gemini MV, at the boundary between Units 4 and 5, a large
350 concave extrusion (up to 800 meters wide and 40 ms TWT deep) is observed (Fig. 5). A channel is
351 present along the PDE and Gemini MV, although the appearance is different. Along the Gemini MV,
352 the channel is very wide (about 800 meters and 20 ms TWT deep) at the base. During deposition of
353 the upper subunit (5c), incision into the underlying deposits along the mud volcano is observed (Fig.
354 5). Along the PDE, a small channel (200 meters wide and 10 ms TWT deep) is present SSW of the
355 heart-shaped deposits within the lower two subunits (5a and b). Within the upper subunit (5c), a
356 wide channel (about 1 km wide and about 25 ms TWT deep) is present along the PDE (Fig. 6). Along
357 the northern part of the PDE, a second channel has developed just southwest of the mounds at the
358 base of the PDE. This channel is 150 meters wide and up to 15 ms TWT deep. Southwest of this
359 second channel, mounded sediments are observed which pass into conformable deposits. In total, 3
360 subunits have been discerned based on small angular unconformities. All subunits consist of high
361 amplitude, continuous reflectors. In Fig. 7, the subunits were again not discernable due to the
362 decreases thickness (Fig. 8). Thicknesses are slighter bigger than unit 4: on average 50 to 55 ms TWT
363 (Fig.8). The mound displays remarkable seismic features: its WSW side contains chaotic, very low-
364 amplitude reflections, while its ENE side displays short horizontal, continuous reflections which seem
365 to be a prolongation of the underlying sedimentation.

366 5. Discussion

367 5.1 Sedimentary processes

368 5.1.1 Initiation (Unit 1)

369 The deposits of Unit 1 drape the basin-boundary and gently level the deepest regions. Settling of
370 sedimentary particles in absence of strong currents, resulting in (hemi-)pelagic deposits (depending
371 on the amount of biogenic material), is proposed as the depositional mechanism. Unit 1 and the base
372 of Unit 2 are affected by faults: several smaller faults at the flanks of the palaeohigh and a large
373 normal fault in the middle of the basin. This faults may be due to the compressional regime in the
374 region (Van Rensbergen et al., 2005). However, as there is only one profile showing these features,
375 they cannot be mapped and as a consequence, the real orientation and direction cannot be derived.
376 The palaeohigh resembles the compressional tectonic ridges (Vernadsky, Renard) and may also be a
377 compressional ridge that did not reach the seafloor and is covered by sediments as a consequence.

378 5.1.2 Sheeted drift (Unit 2)

379 From Unit 2 onwards, very gradually, a contourite drift is being constructed, perpendicular to the
380 margin, with sheeted and detached mounded drift deposits.

381 Unit 2 mostly consists of horizontal, continuous, slightly mounded deposits. Only along the northern
382 part of the PDE, the mounded nature is absent. This mounded nature increases towards the top of
383 the unit (Figs. 5, 6) and indicates together with the fairly uniform thickness perpendicular to the PDE
384 and Gemini MV (Fig. 8), the aggradational stacking pattern and the location along a steep slope
385 towards slope sheeted drift deposits (Faugères and Stow, 2008). Theoretically, sheeted drifts are
386 associated to velocities below 10 cm/s (Stow et al., 2008). The presence of pinched deposits,
387 onlapping onto the PDE within the entire unit suggests a syn-lift sedimentation, affected by the uplift
388 of the PDE, as suggested by Van Rooij et al. (2011). This process diminishes the thickness of the unit
389 in this part of the drift (Figs. 6, 8). The pinch-out diminishes towards the top of the unit and is absent
390 above D2, meaning that the uplift of the PDE stopped at D2. This is not the case near Gemini MV,
391 where a Christmas-tree structure is present, protruding into most of the units (2 to 5), similar to
392 profiles presented in Praeg et al. (2009), Somoza et al. (2003) and Somoza et al. (2012). Periodic mud

393 extrusion from the mud volcano is responsible for this phenomenon, with the largest mud intrusion
394 observed within the upper part of Unit 4 (Fig. 5). After the extrusions, the Pen Duick drift covers the
395 mud with concave deposits (Fig. 5).

396 5.1.3 Mounded drift: Units 3-5

397 Within the sedimentary sequence, the most striking change is the evolution from horizontal, slightly
398 mounded (and along the PDE pinched-out) deposits (Unit 2) into upslope prograding, mounded
399 deposits with a moat (the observed channel) along the PDE and Gemini MV (Units 3 to 5, Figs. 5, 6).
400 Mounded drifts are associated to velocities between 10 and 30 cm/s (Stow et al., 2008), meaning
401 that the inferred bottom current velocities are higher than those present during the deposition of
402 Unit 2. The bottom current strength also increases during the deposition of Unit 3, especially along
403 the southern part of the PDE as the depth of the moat (5 to 20 ms TWT) and the expression of the
404 associated sediment drift mound increases (Figs. 5, 6). This can be interpreted as the evolution from
405 the initiation of mounded drifts towards a continuous bottom current intensity within the moat,
406 gradually leading to erosive (upper parts of Unit 3) instead of non-depositional action (lower parts of
407 Unit 3). Along the northern part of the PDE, a moat and mounded sediments are absent and (hemi-)
408 pelagic sedimentation is present (Fig. 7). This can be interpreted as a lateral decline in bottom
409 current strength, which in this region are not able to create drift deposits. The decline in thickness of
410 Unit 3 (Fig. 8) from southeast to northwest illustrates the lateral change in sedimentation pattern:
411 mounded drift deposits are thicker and occur in the southeastern part and pelagic sediments are
412 thinner and occur in the northwest.

413 Three mound-like structures, originating at the same stratigraphic level, have been observed within
414 Unit 3 in Figure 7. They closely resemble buried CWC mounds discussed by Huvenne et al. (2003),
415 Iacono et al. (accepted) and van Weering et al. (2003) and are classified as such as a consequence.
416 The occurrence of CWC mounds in this part of the study area implies that environmental conditions

417 (food supply, prevention to burial) were right during at least a certain amount of time for CWC to
418 flourish (Foubert et al., 2008; Wienberg et al., 2010; Wienberg et al., 2009).

419 An erosive boundary separates Units 3 and 4 (Figs. 6, 7). Unit 4 is characterized by a larger (and along
420 Gemini MV wider) moat, except for the northern part of the PDE. In this area, the moat is still absent,
421 indicating the continuing lateral decline in bottom current intensity. The erosive nature of the moat
422 indicates faster bottom currents, capable of eroding more sediment. The wider moat along the
423 Gemini MV might indicate a less focussed bottom current. A large mud extrusion is observed at the
424 base of subunit 4c (Fig. 5). This has the same seismic characteristics as and is positioned at the same
425 stratigraphic level as the triangular deposits in Fig. 6. The similarities between both and its position
426 near the Gemini MV indicate a muddy origin for the triangular deposits as well, extruded at the same
427 period. The separate patches of mud (Fig. 2) can be due to two different pathways, certainly as
428 Gemini MV actually consists of two mud volcanoes within one mud cone (Van Rensbergen et al.,
429 2005). The thickness maps (Fig. 8) clearly show the position of the mud extrusion. After the large
430 mud extrusion, the depocenter shifted SSW-wards, hinted by the relocation (about 500 meters) of
431 the moat and mounded sediments (Figs. 5, 6). Along the Gemini MV, this relocation only happens at
432 the base of Unit 5, along the PDE this happens already within subunit 4c.

433 Unit 5 consists of elongate mounded drift deposits along both topographies, even along the northern
434 part of the PDE (Figs.5, 6 and 7). This indicates focussed bottom currents along the entire PDE, strong
435 enough to create drift deposits. A broad and deep moat is present during the deposition of Unit 5.
436 Along the Gemini MV, the moat is at its widest (about 500 meters) of the entire Pen Duick drift,
437 which hints towards a less focussed bottom current, compared to previous units (Fig. 5). Only within
438 the present seafloor, a narrow, deep moat is present directly SSW of the Gemini MV again and is
439 accompanied by a shift in depocenter (Fig. 5). Along the PDE, a narrow but deep moat is present
440 about 500 meters SSW of the escarpment (Fig. 6). Also here, within the present seafloor, the position
441 of the moat shifted to the foot of the PDE.

442 The occurrence of semi-buried CWC mound, recognized at the base of the northern part of the PDE,
443 is a most peculiar feature (Fig. 7). In morphology (width, height, shape) they resemble the CWC
444 mounds found on top of the PDE (Foubert et al., 2008; Van Rooij et al., 2011). However, the presence
445 of continuous reflectors facing the PDE side of these mounded features, resembling the
446 sedimentation below, contradicts a 100% CWC origin. Given the fact that the WSW part of the
447 mound contains a seismic facies resembling the buried mounds of Unit 3 (Fig. 7) and the ENE part
448 contains continuous, parallel, horizontal reflectors, a dual origin for the mounds is proposed. CWC
449 started to settle at the base of the PDE and initiated mound growth. They build a mound against
450 which sediment was deposited, provided by the bottom current along the PDE (inset Fig. 9). This
451 created the mounds, consisting of both a sedimentary (ENE) and CWC mound (WSW) part. This
452 implies that conditions for CWC to thrive were favourable at the foot of the PDE in this region.
453 Unfortunately, further investigations are required to further reveal and understand the exact nature
454 and origin of these features. A small moat along the WSW part of the mounds implies a bottom
455 current flowing along them. Probably due to the presence of these mounds, the depocentre shifted
456 to the WSW and separated mounded drift deposits are present to the WSW (Fig. 7). Whether the
457 bottom current flowing along the Gemini MV and PDE splits or a second bottom current, unrelated to
458 the first one, is present cannot be derived from these profiles (Fig. 2).

459 **5.2 Chronostratigraphy**

460 The spatial and temporal distribution of the Pen Duick contourite drift indicates a depositional
461 history including several changes in sedimentation patterns. Two major (D1, D2) and two minor
462 transitions (D3, D4) are recorded as unconformities separating the depositional sequences. D1 is
463 initiation of drift deposit, D2 marks the transition from sheeted to elongated mounded drifts,
464 whereas D3 and D4 indicate changes within the elongated mounded drift deposits. These alterations
465 have been compared to surrounding regions in order to derive a possible chronostratigraphy. Maad
466 et al. (2010) discussed the seismic stratigraphy of the northwestern Moroccan Atlantic continental

467 shelf based on sparker seismic data. Their unit Q2 is considered to have a Middle to Upper
468 Pleistocene age (correlation with well LAR-A1, 25 km east-southeast of the research area).
469 Correlation (through connecting seismic profiles) of this unit to the investigated region reveals that at
470 least units 3, 4 and 5 are within that age range.

471 Petrographic studies of mud breccia clasts show that the Al Idrissi mud volcano field is situated on an
472 Upper Miocene-Pliocene sedimentary basin (Akhmanov et al., 2003; Pinheiro et al., 2003), implying
473 that the sedimentary deposits described in this paper are of Plio-Pleistocene age. The mud volcanoes
474 appeared 2.4 Ma ago (Van Rensbergen et al., 2005) or 2.6 Ma according to Perez-Garcia et al. (2011),
475 implying that the entire contourite drift (Units 2 to 5) is post-Pliocene in age and only Unit 1 has a
476 possible Pliocene age. Moreover, the basal unconformity, discussed by Van Rensbergen et al. (2005)
477 and Perez-Garcia et al. (2011), is set at an age of 2.6 Ma and agrees to D1. This means that
478 discontinuity D1 could be associated to the BQD (base Quaternary discontinuity), set at 2.588 Ma
479 (Gibbard et al., 2010).

480 During the Quaternary, the Middle Pleistocene Revolution is the most important oceanographic
481 change in the Gulf of Cadiz (and by extension, the entire North-Atlantic), coeval with the switch to a
482 “full” glacial mode with 100 ky eccentricity cyclicity (Cacho et al., 2000; Frigola et al., 2008;
483 Hernández-Molina et al., 2011; Llave et al., 2007; Llave et al., 2006). Changes in water mass
484 circulation and marine sedimentation patterns, mostly evidenced by higher amplitude reflectors and
485 more vigorous current patterns, are observed in the Gulf of Cadiz (Hernández-Molina et al., 2006b;
486 Llave et al., 2007), the Cantabrian margin (Van Rooij et al., 2010) and the Porcupine Seabight (Van
487 Rooij et al., 2007). A similar observation has been made here: a switch from sheeted to elongate
488 mounded drift deposits and a gradual increase in amplitudes of the reflections throughout Units 3, 4
489 and 5 (Figs. 5, 6, 7). Therefore, discontinuity D2 may be correlated to the MPR (0.920 Ma).

490 Continental shelves and upper slopes are more prone to eustatic variations compared to deep-water
491 environments and in response, bottom currents fluctuate more in these regions (Hernández-Molina

492 et al., 2002; Ridente et al., 2009; Verdicchio and Trincardi, 2008). The upper three units display
493 features which can be attributed to climatic variations: a cyclic pattern of progradational (onto the
494 PDE or Gemini MV) subunits with reflectors of varying amplitudes. As the majority (65-80%) of the
495 sediment is deposited during regressive and lowstand periods in the Gulf of Cadiz and the Alboran
496 Sea (Hernández-Molina et al., 2002), the subunits can be tentatively linked to glacial marine isotopic
497 stages (MIS). This correlation has been applied before along the Adriatic margin by Ridente et al.
498 (2009) and along the southwestern Mallorca shelf by Vandorpe et al. (2011). The ten discerned
499 subunits from the MPR to Recent can be correlated to the ten (even) MIS (Lisiecki and Raymo, 2005)
500 (Figs. 5, 6). A periodicity of 80 to 120 ky is obtained due to this correlation, which is in agreement
501 with the obliquity pacing hypothesis proposed by Huybers and Wunsch (2005) and Huybers (2007),
502 stating that glacial cycles vary by 80 or 120 ky in the late-Pleistocene by skipping one or two obliquity
503 beats. As a result, D3 and D4 are linked to MIS 15 (about 575 ka) and 9 (about 325 ka) respectively.
504 At 575 ka, an intensification of the bottom current regime occurred in the area, evidenced by larger
505 moat (Figs. 5, 6). At 325 ka, a defocussing occurred, leading to a wider, less deep moat (Figs. 5, 6).

506 Based on this chronostratigraphy and the average measured thicknesses (conversion into meters
507 based on a theoretical seismic velocity of 1650 m/s within the sediment), the sedimentation rate for
508 the period between BQD and MPR (Unit 2) is 10.8 cm/ky and between MPR and Recent (Units 3 to 5)
509 17.0 cm/ky. These rates are close to or within the range of theoretical values for sediment drifts: 3-
510 10 cm/ky for sheeted drifts (Unit 2) and 5-30 cm/ky for mounded drifts (Units 3 to 5) (Stow et al.,
511 2008). Also, the increase in sedimentation rate after the MPR is consistent with the enhanced
512 sedimentation rates observed in the Cadiz CDS in the north (Llave et al., 2001; Llave et al., 2011) and
513 the Le Danois CDS (Van Rooij et al., 2010).

514 **5.3 Comparison to the northern Gulf of Cadiz palaeoceanography**

515 When comparing the depositional history of the Pen Duick contourite drift to other systems along
516 the eastern boundary of the North Atlantic (Cadiz and Le Danois CDS), several resemblances and

517 differences can be identified. While in the Cadiz and Le Danois CDS, drift deposits are present from
518 the Pliocene onwards, the PDE area only contains Quaternary drift deposits. After the MPR, an
519 intensification of bottom currents and an accompanying growth of the CDS occurs in all drift systems,
520 expressed by a severe growth phase of the mounded drift deposits in the Cadiz and Le Danois areas
521 (Llave et al., 2011; Roque et al., 2012; Van Rooij et al., 2010) and by the evolution from sheeted to
522 mounded drift deposits in the PDE area (Figs. 5, 6). A final intensification stage is observed in the
523 Cadiz CDS around MIS 12 (Llave et al., 2001; Llave et al., 2007; Llave et al., 2011; Marchès et al., 2010;
524 Roque et al., 2012), while in the Pen Duick drift, this intensification is tentatively set at MIS 15. The
525 boundary at MIS 9 observed in the Pen Duick drift is not encountered in the other systems.

526 The vast differences in evolution between MOW-controlled CDS's and the Pen Duick contourite drift
527 indicates that MOW is not likely to be involved in the formation or shaping of the Pen Duick drift.
528 Although the MOW is present within the area as meddies (Ambar et al., 2008), along the PDE it is not
529 observed (Only in deeper water settings, Fig. 3). During glacial periods, MOW flows at even greater
530 depths (García et al., 2009) and therefore, its presence at the foot of the PDE during glacials is not
531 likely as well. AAIW enters the Gulf of Cadiz in the south and flows along the African coast towards
532 the north, before being outcompeted by the MOW (Louarn and Morin, 2011; Machín et al., 2006a).
533 CTD data from Van Rooij et al. (2011) and Mienis et al. (2012) indicate the presence of AAIW at the
534 foot of the escarpment, while NACW is present on top. The absence of MOW, the proved presence of
535 AAIW and the depth range in which the Pen Duick drift occurs favours towards an AAIW-origin and
536 would make it the most northern contourite drift in the Atlantic Ocean with a possible AAIW-origin.

537 Mienis et al. (2012) showed the presence of northeast-directed currents at the foot of the PDE. This
538 is in agreement with the observed seismic characteristics and geomorphology of the Pen Duick drift.
539 A moat is present along the PDE and Gemini MV, indicating a bottom current along both
540 topographies. This bottom current has been active throughout the entire Quaternary (Figs. 5, 6 and
541 7), depositing sediment SSW of the Gemini MV and PDE. Taking into account the pathway of the

542 bottom current and the Coriolis deflection to the right in the northern hemisphere, the bottom
543 current is inferred to have an northeastward direction. The pathway of the AAIW, the CTD data and
544 the flow direction at the foot of the topographies together hint towards a bottom current coming
545 from the south (most likely an AAIW-origin), being deflected by the Gemini MV and PDE and which
546 continues to flow along the bases of the topographies due to Coriolis deflection. The start of drift
547 formation (Unit 2, Figs. 5, 6) 2.588 Ma ago coincides with the first signs of mud eruption and the
548 initial uplift of the PDE (Perez-Garcia et al., 2011; Van Rensbergen et al., 2005). So, only when the
549 Gemini MV and PDE rose high enough to alter the bottom current pattern and possibly speed them
550 up (Faugères et al., 1999), the Pen Duick contourite drift started to form. Higher velocities due to
551 small-scale topographies (such as seamounts, mud volcanoes, escarpments, ...) are commonly
552 described (Hernández-Molina et al., 2011; Rebesco et al., submitted; Stow et al., 2009). Taking into
553 account the fact that bottom currents are on average 8 cm/s on the plain at the foot of the PDE
554 (Mienis et al., 2012) and that drift deposits solely occur along the topographies, the Pen Duick
555 contourite drift is an excellent example of an obstacle-related contourite system.

556 **6. Conclusions**

557 Based on sparker single-channel seismic, an airgun multi-channel seismic and multibeam data, a
558 contourite drift along the southwestern border of the Pen Duick escarpment and Gemini mud
559 volcano has been described in terms of sedimentary evolution and palaeoceanography. Five
560 conclusions can be drawn from this study:

- 561 1. The Pen Duick contourite drift is an excellent example of an obstacle-related drift as it occurs in
562 an area with in general low bottom-currents. Bottom currents are deflected against the
563 topographies (PDE and Gemini MV) and build a contourite drift along them, perpendicular to the
564 continental margin.
- 565 2. The Pen Duick contourite drift originates at the base of the Quaternary, creating sheeted drift
566 deposits (Unit 2). Bottom currents intensify after the MPR, leading to the deposition of separated

567 mounded drift deposits (Unit 3 to 5). A general intensification of bottom currents is inferred from
568 the MPR to present

569 3. The presence of the Gemini MV interferes with the drift deposits: several extrusions are recorded
570 within the sedimentary sequence leading to a Christmas-tree structure along the mud volcano.

571 The presence of a large block of mud along both PDE and Gemini MV within unit 4 indicates a
572 large eruption in that period.

573 4. The Pen Duick contourite drift has a possible AAIW-origin which makes would make it the most
574 northern expression of AAIW within the Atlantic Ocean. Evidence (both seismic and CTD) for the
575 presence of MOW at the foot of the PDE is not present.

576 5. CWC mounds have been found within and on top of the northern part of the Pen Duick drift. This
577 means that not only on top of the PDE, environmental conditions were right for CWC to flourish,
578 but also at its base. The presence of the buried mounds indicates that also in the past, conditions
579 were favourable for CWC mound growth.

580 **7. Acknowledgments**

581 The authors would like to acknowledge the captains and crews of R/V Belgica and R/V Pelagia for the
582 many successful cruises to the study area. The helpful and stimulating discussions with J.-P. Henriët
583 (UGent) and F.J. Hernández-Molina (U. Vigo) are greatly appreciated. The data was acquired within
584 the framework of the following past projects: ESF EuroDIVERSITY MICROSISTEMS, ESF EuroMARGINS
585 MoundForce, EC FP6 HERMES (GOCE-CT-2005-511234) and EC FP7 IP HERMIONE (Grant agreement
586 n°226354). The aims and strategies of this paper were elaborated within the framework of the FWO-
587 Flanders project "CONTOURITE-3D", as well as IGCP project 619 and INQUA project 1204. Finally, we
588 wish to thank the reviewers for their helpful comments.

589 **8. References**

590 World Ocean Database, 05/02/2013. http://www.nodc.noaa.gov/OC5/WOD09/pr_wod09.html.

591

592 Akhmanov, G., Ivanov, M., Henriot, J.P., Sarantzev, E.S., 2003. The El Arraiche mud volcano field and
593 its "exotic" mud volcano deposits recovered during the TTR-12 cruise in the Gulf of Cadiz, in: Marani,
594 M., Akhmanov, G., Suzyumov, A. (Eds.), Geological and biological processes at deep-sea European
595 margins and oceanic basins. UNESCO, Bologna, Italy, pp. 9-10.

596

597 Ambar, I., Serra, N., Neves, F., Ferreira, T., 2008. Observations of the Mediterranean Undercurrent
598 and eddies in the Gulf of Cadiz during 2001. *Journal of Marine Systems* 71, 195-220.

599

600 Antich, N., Buitrago, J., García Mojónero, C., Jiménez, A., Martínez del Olmo, W., 2005. Contourites:
601 An unknown and excellent reservoir (Gulf of Cadiz, SW Spain). 25 aniversario de la Asociación de
602 Geólogos Geofísicos Españoles del Petróleo AAGGEP, Spec. Publ., 75-82.

603

604 Cacho, I., Grimalt, J.O., Sierro, F.J., Shackleton, N., Canals, M., 2000. Evidence for enhanced
605 Mediterranean thermohaline circulation during rapid climatic coolings. *Earth and Planetary Science*
606 *Letters* 183, 417-429.

607

608 Criado-Aldeanueva, F., García-Lafuente, J., Vargas, J.M., Del Río, J., Vázquez, A., Reul, A., Sánchez, A.,
609 2006. Distribution and circulation of water masses in the Gulf of Cadiz from in situ observations.
610 *Deep Sea Research Part II: Topical Studies in Oceanography* 53, 1144-1160.

611

612 Dalrymple, R.W., LeGresley, E.M., Fader, G.B.J., Petrie, B.D., 1992. The western Grand Banks of
613 Newfoundland: Transgressive Holocene sedimentation under the combined influence of waves and
614 currents. *Marine Geology* 105, 95-118.

615

616 De Mol, L., Hilário, A., Van Rooij, D., Henriët, J.P., 2011. Habitat mapping of a cold-water coral mound
617 on Pen Duick escarpment (Gulf of Cadiz), in: Harris, P., Baker, E. (Eds.), Seafloor morphology as
618 benthic habitat. Elsevier, pp. 645-654.

619

620 Duarte, C.S.L., Viana, A.R., 2007. Santos Drift System: stratigraphic organization and implications for
621 late Cenozoic palaeocirculation in the Santos Basin, SW Atlantic Ocean. Geological Society, London,
622 Special Publications 276, 171-198.

623

624 Expedition 339 Scientists, 2012. Mediterranean outflow: environmental significance of the Mediterranean
625 Outflow Water and its global implications. *IODP Prel. Rept.*, 339. doi:10.2204/iodp.pr.339.2012

626 Faugères, J.-C., Stow, D.A.V., Imbert, P., Viana, A., 1999. Seismic features diagnostic of contourite
627 drifts. *Marine Geology* 162, 1-38.

628

629 Faugères, J., Stow, D.A.V., 1993a. Bottom-current-controlled sedimentation: A synthesis of the
630 contourite problem. *Sedimentary Geology* 82.

631

632 Faugères, J.C., Stow, D.A.V., 1993b. Contourite drift types and their distribution in the North and
633 South Atlantic Ocean basins. *Sedimentary Geology* 82, 189-203.

634

635 Faugères, J.C., Stow, D.A.V., 2008. Contourite drifts: Nature, Evolution and Controls, in: Rebesco, M.,
636 Camerlenghi, A. (Eds.), Contourites. Elsevier, pp. 259-288.

637 Flinch, J.F., 1993. Tectonic evolution of the Gibraltar Arc. Rice University, Houston, Texas, p. 381.

638

639 Foubert, A., Depreiter, D., Beck, T., Maignien, L., Pannemans, B., Frank, N., Blamart, D., Henriët, J.-P.,
640 2008. Carbonate mounds in a mud volcano province off north-west Morocco: Key to processes and
641 controls. *Marine Geology* 248, 74-96.

642
643
644
645
646
647
648
649
650
651
652
653
654
655
656
657
658
659
660
661
662
663
664
665
666
667

Frank, N., Ricard, E., Lutringer-Paquet, A., van der Land, C., Colin, C., Blamart, D., Foubert, A., Van Rooij, D., Henriët, J.-P., de Haas, H., van Weering, T., 2009. The Holocene occurrence of cold water corals in the NE Atlantic: Implications for coral carbonate mound evolution. *Marine Geology* 266, 129-142.

Frigola, J., Moreno, A., Cacho, I., Canals, M., Sierro, F.J., Flores, J.A., Grimalt, J.O., 2008. Evidence of abrupt changes in Western Mediterranean Deep Water circulation during the last 50 kyr: A high-resolution marine record from the Balearic Sea. *Quaternary International* 181, 88-104.

García, M., 2002. Caracterización morfológica del sistema de canales y valles submarinos del talud medio del Golfo de Cádiz (SO de la Península Ibérica): Implicaciones oceanográficas., Facultad de Ciencias de l Mar. Univ. Cádiz, Cádiz, p. 114.

García, M., Hernández-Molina, F.J., Llave, E., Stow, D.A.V., León, R., Fernández-Puga, M.C., Díaz del Río, V., Somoza, L., 2009. Contourite erosive features caused by the Mediterranean Outflow Water in the Gulf of Cadiz: Quaternary tectonic and oceanographic implications. *Marine Geology* 257, 24-40.

Gibbard, P.L., Head, M.J., Walker, M.J.C., 2010. Formal ratification of the Quaternary System/Period and the Pleistocene Series/Epoch with a base at 2.58 Ma. *Journal of Quaternary Science* 25, 96-102.

Haffert, L., Haeckel, M., Liebetrau, V., Berndt, C., Hensen, C., Nuzzo, M., Reitz, A., Scholz, F., Schönfeld, J., Perez-Garcia, C., Weise, S.M., 2013. Fluid evolution and authigenic mineral paragenesis related to salt diapirism – The Mercator mud volcano in the Gulf of Cadiz. *Geochimica et Cosmochimica Acta* 106, 261-286.

668 Hans Nelson, C., Baraza, J., Maldonado, A., 1993. Mediterranean undercurrent sandy contourites,
669 Gulf of Cadiz, Spain. *Sedimentary Geology* 82, 103-131.
670

671 Haq, B.U., Hardenbol, J., Vail, P.R., 1987. Chronology of Fluctuating Sea Levels Since the Triassic.
672 *Science* 235, 1156-1167.
673

674 Heezen, B.C., Hollister, C.D., Ruddiman, W.F., 1966. Shaping of the continental rise by deep
675 geostrophic currents. *Science* 152, 502-508.
676

677 Hernández-Molina, F.J., Larter, R.D., Rebesco, M., Maldonado, A., 2006a. Miocene reversal of bottom
678 water flow along the Pacific Margin of the Antarctic Peninsula: Stratigraphic evidence from a
679 contourite sedimentary tail. *Marine Geology* 228, 93-116.
680

681 Hernández-Molina, F.J., Llave, E., Stow, D.A.V., García, M., Somoza, L., Vázquez, J.T., Lobo, F.J.,
682 Maestro, A., Díaz del Río, V., León, R., Medialdea, T., Gardner, J., 2006b. The contourite depositional
683 system of the Gulf of Cádiz: A sedimentary model related to the bottom current activity of the
684 Mediterranean outflow water and its interaction with the continental margin. *Deep Sea Research*
685 *Part II: Topical Studies in Oceanography* 53, 1420-1463.
686

687 Hernández-Molina, F.J., Maldonado, A., Stow, D.A.V., 2008. Abyssal plain contourites, in: Rebesco,
688 M., Camerlenghi, A. (Eds.), *Contourites*. Elsevier, pp. 347-378.
689

690 Hernández-Molina, F.J., Serra, N., Stow, D.A.V., Llave, E., Ercilla, G., Van Rooij, D., 2011. Along-slope
691 oceanographic processes and sedimentary products around the Iberian margin. *Geo-Mar Lett* (in
692 press).
693

694 Hernández-Molina, F.J., Somoza, L., Vazquez, J.T., Lobo, F., Fernández-Puga, M.C., Llave, E., Díaz-del
695 Río, V., 2002. Quaternary stratigraphic stacking patterns on the continental shelves of the southern
696 Iberian Peninsula: their relationship with global climate and palaeoceanographic changes.
697 Quaternary International 92, 5-23.
698

699 Huvenne, V.A.I., De Mol, B., Henriët, J.P., 2003. A 3D seismic study of the morphology and spatial
700 distribution of buried coral banks in the Porcupine Basin, SW of Ireland. Marine Geology 198, 5-25.

701 Huybers, P., 2007. Glacial variability over the last two million years: an extended depth-derived
702 agemodel, continuous obliquity pacing, and the Pleistocene progression. Quaternary Science Reviews
703 26, 37-55.
704

705 Huybers, P., Wunsch, C., 2005. Obliquity pacing of the late Pleistocene glacial terminations. Nature
706 434, 491-494.
707

708 Iacono, C.L., Gràcia, E., Ranero, C.R., Emelianov, M., Huvenne, V., Bartolomé, R., Booth-Rea, G.,
709 Prades, J., the Melcor Cruise Party, accepted. The West Melilla Cold Water Coral Mounds, Eastern
710 Alboran Sea: Morphological characterization and environmental context. Deep Sea Research Part II:
711 Topical Studies in Oceanography.
712

713 Lisiecki, L.E., Raymo, M.E., 2005. A Plio-Pleistocene stack of 57 globally distributed benthic delta 18O
714 records. Paleoceanography 20, PA1003.
715

716 Llave, E., Hernández-Molina, F.J., Somoza, L., Díaz-del-Río, V., Stow, D.A.V., Maestro, A., Alveirinho
717 Dias, J.M., 2001. Seismic stacking pattern of the Faro-Albufeira contourite system (Gulf of Cadiz): a
718 Quaternary record of paleoceanographic and tectonic influences. Marine Geophysical Research 22,
719 487-508.

720

721 Llave, E., Hernández-Molina, F.J., Somoza, L., Stow, D.A.V., Díaz Del Río, V., 2007. Quaternary
722 evolution of the contourite depositional system in the Gulf of Cadiz. Geological Society, London,
723 Special Publications 276, 49-79.

724

725 Llave, E., Hernández-Molina, F.J., Stow, D.A.V., Somoza, L., Díaz-del-Río, V., 2005. The contourite
726 depositional system in the Gulf of Cadiz: an example of drifts with reservoir potential characteristics.
727 25 aniversario de la Asociación de Geólogos Geofísicos Españoles del Petróleo AAGGEP, Spec. Publ.,
728 53-73.

729

730 Llave, E., Matias, H., Hernández-Molina, F., Ercilla, G., Stow, D., Medialdea, T., 2011. Pliocene–
731 Quaternary contourites along the northern Gulf of Cadiz margin: sedimentary stacking pattern and
732 regional distribution. *Geo-Marine Letters* 31, 377-390.

733

734 Llave, E., Schönfeld, J., Hernández-Molina, F.J., Mulder, T., Somoza, L., Díaz del Río, V., Sánchez-
735 Almazo, I., 2006. High-resolution stratigraphy of the Mediterranean outflow contourite system in the
736 Gulf of Cadiz during the late Pleistocene: The impact of Heinrich events. *Marine Geology* 227, 241-
737 262.

738

739 Locker, S.D., Laine, E.P., 1992. Paleogene-Neogene depositional history of the middle U.S. Atlantic
740 continental rise: mixed turbidite and contourite depositional systems. *Marine Geology* 103, 137-164.

741

742 Louarn, E., Morin, P., 2011. Antarctic Intermediate Water influence on Mediterranean Sea Water
743 outflow. *Deep Sea Research Part I: Oceanographic Research Papers* 58, 932-942.

744

745 Lowrie, A., 1986. Model for fine-scale movements associated with climate and sea level changes
746 along the Louisiana shelfbreak growth faults. Gulf Coast Association Geological Societies Transactions
747 36, 497-508.
748

749 Maad, N., Le Roy, P., Sahabi, M., Gutscher, M.-A., Hssain, M., Babonneau, N., Rabineau, M., Lanoë,
750 B.V.V., 2010. Seismic stratigraphy of the NW Moroccan Atlantic continental shelf and Quaternary
751 deformation at the offshore termination of the southern Rif front. Comptes Rendus Geoscience 342,
752 731-740.
753

754 Machín, F., Hernández-Guerra, A., Pelegrí, J.L., 2006a. Mass fluxes in the Canary Basin. Progress In
755 Oceanography 70, 416-447.
756

757 Machín, F., Pelegrí, J.L., Marrero-Díaz, A., Laiz, I., Ratsimandresy, A.W., 2006b. Near-surface
758 circulation in the southern Gulf of Cádiz. Deep Sea Research Part II: Topical Studies in Oceanography
759 53, 1161-1181.
760

761 Maldonado, A., Somoza, L., Pallarés, L., 1999. The Betic orogen and the Iberian-African boundary in
762 the Gulf of Cadiz: geological evolution (central North Atlantic). Marine Geology 155, 9-43.
763

764 Marchès, E., Mulder, T., Gonthier, E., Cremer, M., Hanquiez, V., Garlan, T., Lecroart, P., 2010. Perched
765 lobe formation in the Gulf of Cadiz: Interactions between gravity processes and contour currents
766 (Algarve Margin, Southern Portugal). Sedimentary Geology 229, 81-94.
767

768 Mccave, I.N., Tucholke, B.E., 1986. Deep current-controlled sedimentation in the western North
769 Atlantic, in: McCreggor, B.A. (Ed.), The western North Atlantic region. The geological society of
770 America, pp. 451-468.

771

772 Medialdea, T., Somoza, L., Pinheiro, L.M., Fernández-Puga, M.C., Vázquez, J.T., León, R., Ivanov, M.K.,
773 Magalhaes, V., Díaz-del-Río, V., Vegas, R., 2009. Tectonics and mud volcano development in the Gulf
774 of Cádiz. *Marine Geology* 261, 48-63.

775

776 Medialdea, T., Vegas, R., Somoza, L., Vázquez, J.T., Maldonado, A., Díaz-del-Río, V., Maestro, A.,
777 Córdoba, D., Fernández-Puga, M.C., 2004. Structure and evolution of the "Olistostrome" complex of
778 the Gibraltar Arc in the Gulf of Cádiz (eastern Central Atlantic): evidence from two long seismic cross-
779 sections. *Marine Geology* 209, 173-198.

780

781 Mienis, F., De Stigter, H.C., De Haas, H., Van der Land, C., Van Weering, T.C.E., 2012. Hydrodynamic
782 conditions in a cold-water coral mound area on the Renard Ridge, southern Gulf of Cadiz. *Journal of*
783 *Marine Systems* 96–97, 61-71.

784

785 Millot, C., 2009. Another description of the Mediterranean Sea outflow. *Progress In Oceanography*
786 82, 101-124.

787

788 Perez-Garcia, C., Berndt, C., Klaeschen, D., Mienert, J., Haffert, L., Depreiter, D., Haeckel, M., 2011.
789 Linked halokinesis and mud volcanism at the Mercator mud volcano, Gulf of Cadiz. *Journal of*
790 *Geophysical Research: Solid Earth* 116, n/a-n/a.

791

792 Pinheiro, L.M., Ivanov, M.K., Sautkin, A., Akhmanov, G., Magalhães, V.H., Volkonskaya, A., Monteiro,
793 J.H., Somoza, L., Gardner, J., Hamouni, N., Cunha, M.R., 2003. Mud volcanism in the Gulf of Cadiz:
794 results from the TTR-10 cruise. *Marine Geology* 195, 131-151.

795

796 Pirlet, H., Wehrmann, L.M., Brunner, B., Frank, N., Dewanckele, J.A.N., Van Rooij, D., Foubert, A.,
797 Swennen, R., Naudts, L., Boone, M., Cnudde, V., Henriët, J.-P., 2010. Diagenetic formation of gypsum
798 and dolomite in a cold-water coral mound in the Porcupine Seabight, off Ireland. *Sedimentology* 57,
799 786-805.
800
801 Praeg, D., Ceramicola, S., Barbieri, R., Unnithan, V., Wardell, N., 2009. Tectonically-driven mud
802 volcanism since the late Pliocene on the Calabrian accretionary prism, central Mediterranean Sea.
803 *Marine and Petroleum Geology* 26, 1849-1865.
804
805 Preu, B., Hernández-Molina, F.J., Violante, R., Piola, A.R., Paterlini, C.M., Schwenk, T., Voigt, I.,
806 Krastel, S., Spiess, V., 2013. Morphosedimentary and hydrographic features of the northern
807 Argentine margin: The interplay between erosive, depositional and gravitational processes and its
808 conceptual implications. *Deep Sea Research Part I: Oceanographic Research Papers* 75, 157-174.
809
810 Rebesco, M., Hernández-Molina, F.J., van Rooij, D., Wåhlin, A., submitted. Contourites and associated
811 sediments controlled by deep-water circulation processes: State of the art and future considerations.
812 *Marine Geology*.
813
814 Rebesco, M., Richard, C.S., Cocks, L.R.M., Ian, R.P., 2005. Sedimentary environments: Contourites,
815 *Encyclopedia of Geology*. Elsevier, Oxford, pp. 513-528.
816
817 Richardson, P.L., Bower, A.S., Zenk, W., 2000. A census of Meddies tracked by floats. *Progress In*
818 *Oceanography* 45, 209-250.
819

820 Ridente, D., Trincardi, F., Piva, A., Asioli, A., 2009. The combined effect of sea level and supply during
821 Milankovitch cyclicity: Evidence from shallow-marine $\delta^{18}\text{O}$ records and sequence architecture
822 (Adriatic margin). *Geology* 37, 1003-1006.

823

824 Roque, C., Duarte, H., Terrinha, P., Valadares, V., Noiva, J., Cachão, M., Ferreira, J., Legoinha, P.,
825 Zitellini, N., 2012. Pliocene and Quaternary depositional model of the Algarve margin contourite
826 drifts (Gulf of Cadiz, SW Iberia): Seismic architecture, tectonic control and paleoceanographic
827 insights. *Marine Geology* 303–306, 42-62.

828

829 Schneider, E.D., Fox, P.J., Hollister, C.D., Needham, H.D., Heezen, B.C., 1967. Further evidence of
830 contour currents in the Western North Atlantic. *Earth and Planetary Science Letters* 2, 351-359.

831

832 Somoza, L., Díaz del Río, V., León, R., Ivanov, M., Fernández-Puga, M.C., Gardner, J.M., Hernández-
833 Molina, F.J., Pinheiro, L.M., Rodero, J., Lobato, A., Maestro, A., Vázquez, J.T., Medialdea, T.,
834 Fernández-Salas, L.M., 2003. Seabed morphology and hydrocarbon seepage in the Gulf of Cádiz mud
835 volcano area: Acoustic imagery, multibeam and ultra-high resolution seismic data. *Marine Geology*
836 195, 153-176.

837

838 Somoza, L., Medialdea, T., León, R., Ercilla, G., Vázquez, J.T., Farran, M.I., Hernández-Molina, J.,
839 González, J., Juan, C., Fernández-Puga, M.C., 2012. Structure of mud volcano systems and pockmarks
840 in the region of the Ceuta Contourite Depositional System (Western Alborán Sea). *Marine Geology*
841 332–334, 4-26.

842

843 Stow, D.A.V., Faugères, J.-C., Howe, J.A., Pudsey, C.J., Viana, A.R., 2002. Bottom currents, contourites
844 and deep-sea sediment drifts: current state-of-the-art. Geological Society, London, *Memoirs* 22, 7-20.

845

846 Stow, D.A.V., Hernández-Molina, F.J., 2006. Environmental significance of the Mediterranean outflow
847 water and its global implications, IODP Full Proposal 644.
848

849 Stow, D.A.V., Hernández-Molina, F.J., Llave, E., Sayago, M., Díaz del Río, V., Branson, A., 2009.
850 Bedform-velocity matrix: the estimation of bottom current velocity from bedform observations.
851 *Geology* 37, 327-330.
852

853 Stow, D.A.V., Hunter, S., Wilkinson, D., Hernández-Molina, F.J., 2008. The nature of contourite
854 deposition, in: Rebesco, M., Camerlenghi, A. (Eds.), *Contourites*. Elsevier.
855

856 Templer, S.P., Wehrmann, L.M., Zhang, Y., Vasconcelos, C., McKenzie, J.A., 2011. Microbial
857 community composition and biogeochemical processes in cold-water coral carbonate mounds in the
858 Gulf of Cadiz, on the Moroccan margin. *Marine Geology* 282, 138-148.
859

860 Tingay, M.R.P., Hillis, R.R., Morley, C.K., Swarbrick, R.E., Okpere, E.C., 2003. Pore pressure/stress
861 coupling in Brunei Darussalam — implications for shale injection. Geological Society, London, Special
862 Publications 216, 369-379.
863

864 Toucanne, S., Mulder, T., Schönfeld, J., Hanquiez, V., Gonthier, E., Duprat, J., Cremer, M., Zaragosi, S.,
865 2007. Contourites of the Gulf of Cadiz: A high-resolution record of the paleocirculation of the
866 Mediterranean outflow water during the last 50,000 years. *Palaeogeography, Palaeoclimatology,*
867 *Palaeoecology* 246, 354-366.
868

869 Van Rensbergen, P., Depreiter, D., Pannemans, B., Moerkerke, G., Van Rooij, D., Marsset, B.,
870 Akhmanov, G., Blinova, V., Ivanov, M., Rachidi, M., Magalhaes, V., Pinheiro, L., Cunha, M., Henriët, J.-

871 P., 2005. The El Arraiche mud volcano field at the Moroccan Atlantic slope, Gulf of Cadiz. *Marine*
872 *Geology* 219, 1-17.
873

874 Van Rooij, D., Blamart, D., De Mol, L., Mienis, F., Pirlet, H., Wehrmann, L.M., Barbieri, R., Maignien, L.,
875 Templer, S.P., de Haas, H., Hebbeln, D., Frank, N., Larmagnat, S., Stadnitskaia, A., Stivaletta, N., van
876 Weering, T., Zhang, Y., Hamoumi, N., Cnudde, V., Duyck, P., Henriët, J.P., 2011. Cold-water coral
877 mounds on the Pen Duick Escarpment, Gulf of Cadiz: The MiCROSYSTEMS project approach. *Marine*
878 *Geology* 282, 102-117.
879

880 Van Rooij, D., Blamart, D., Richter, T., Wheeler, A., Kozachenko, M., Henriët, J.P., 2007. Quaternary
881 sediment dynamics in the Belgica mound province, Porcupine Seabight: ice-rafting events and
882 contour current processes. *International Journal of Earth Sciences* 96, 121-140.
883

884 Van Rooij, D., Iglesias, J., Hernández-Molina, F.J., Ercilla, G., Gomez-Ballesteros, M., Casas, D., Llave,
885 E., De Hauwere, A., Garcia-Gil, S., Acosta, J., Henriët, J.P., 2010. The Le Danois Contourite
886 Depositional System: Interactions between the Mediterranean Outflow Water and the upper
887 Cantabrian slope (North Iberian margin). *Marine Geology (2010)* 274, 1-20.
888

889 van Weering, T.C.E., de Haas, H., de Stigter, H.C., Lykke-Andersen, H., Kouvaev, I., 2003. Structure and
890 development of giant carbonate mounds at the SW and SE Rockall Trough margins, NE Atlantic
891 Ocean. *Marine Geology* 198, 67-81.
892

893 Vandorpe, T., Van Rooij, D., Stow, D., Henriët, J.-P., 2011. Pliocene to Recent shallow-water
894 contourite deposits on the shelf and shelf edge off south-western Mallorca, Spain. *Geo-Marine*
895 *Letters* 31, 391-403.
896

897 Verdicchio, G., Trincardi, F., 2008. Shallow-water Contourites, in: Rebesco, M., Camerlenghi, A. (Eds.),
898 Contourites. Elsevier, *Developments in Sedimentology*, pp. 409-433.
899

900 Viana, A.R., Almeida, W., Jr, Nunes, M.C.V., Bulhoes, E.M., 2007. The economic importance of
901 contourites. Geological Society, London, Special Publications 276, 1-23.
902

903 Viana, A.R., Faugères, J.C., Kowsmann, R.O., Lima, J.A.M., Caddah, L.F.G., Rizzo, J.G., 1998a.
904 Hydrology, morphology and sedimentology of the Campos continental margin, offshore Brazil.
905 *Sedimentary Geology* 115, 133-157.
906

907 Viana, A.R., Faugères, J.C., Stow, D.A.V., 1998b. Bottom-current-controlled sand deposits -- a review
908 of modern shallow- to deep-water environments. *Sedimentary Geology* 115, 53-80.
909

910 Wehrmann, L.M., Templer, S.P., Brunner, B., Bernasconi, S.M., Maignien, L., Ferdelman, T.G., 2011.
911 The imprint of methane seepage on the geochemical record and early diagenetic processes in cold-
912 water coral mounds on Pen Duick Escarpment, Gulf of Cadiz. *Marine Geology* 282, 118-137.
913

914 Wienberg, C., Frank, N., Mertens, K.N., Stuut, J.-B., Marchant, M., Fietzke, J., Mienis, F., Hebbeln, D.,
915 2010. Glacial cold-water coral growth in the Gulf of Cádiz: Implications of increased palaeo-
916 productivity. *Earth and Planetary Science Letters* 298, 405-416.
917

918 Wienberg, C., Hebbeln, D., Fink, H.G., Mienis, F., Dorschel, B., Vertino, A., Correa, M.L., Freiwald, A.,
919 2009. Scleractinian cold-water corals in the Gulf of Cádiz—First clues about their spatial and temporal
920 distribution. *Deep Sea Research Part I: Oceanographic Research Papers* 56, 1873-1893.
921

922

923

924 **Figure Captions**

925 Fig. 1: Overview of the oceanic circulation and main geological features within the Gulf of Cadiz. The
926 white dots represent mud volcanoes within the Spanish-Portuguese mud volcano field (SPM) and the
927 white circle with a dot is the Lolita salt diapir. The transparent white box indicates the investigated
928 area (Fig. 2) and the double arrow shows the transect of the CTD profile (Fig. 3). a: Donana diapiric
929 ridge, b: Cadiz diapiric ridge, GDR: Guadalquivir mud volcano field, DPM: Deep Portuguese mud
930 volcano field, UC: MOW upper current, IB: MOW intermediate branch, PB: MOW principal branch,
931 SB: MOW southern branch, MOW: Mediterranean Outflow Water, AAIW: Antarctic Intermediate
932 Water, NACW: North Atlantic Central Water, NADW: North Atlantic Deep Water

933 Fig. 2: Topographic features in the Pen Duick area and location of the discussed seismic profiles. The
934 inset shows the topography perpendicular to the Gemini mud volcano. The black arrows indicate the
935 position of the moats and the inferred direction of the current within them. The white dots indicate
936 the six mounds at the base of the PDE, while the white circles indicate alpha (most southern), beta
937 (central) and gamma (most northern) mound. LdT: Lazarillo del Torres (mud volcano). Multibeam
938 bathymetry discussed by Van Rensbergen et al. (2005).

939 Fig. 3: A) Salinity (colors) and temperature (contours, °C) transect 10-15 km south of the Gemini Mud
940 Volcano and Pen Duick Escarpment (PDE). The data were obtained from the world ocean database
941 (World Ocean Database, 05/02/2013). B) Salinity-temperature plot of used CTD stations. NASW is
942 characterized by high temperature and salinity values, NACW by a decreasing line on the T-S plot and
943 decreasing temperatures and salinities in the transect. AAIW lies on a line of increasing salinities in
944 the transect, is characterized by slightly higher salinity values compared to the NACW. The MOW is
945 characterized by high salinity values (Louarn and Morin, 2011; Machín et al., 2006b).

946 Fig. 4: Multichannel airgun seismic profile (and interpretation) displaying 5 seismic stratigraphic
947 units. Unit 1 and the upper part of Unit 2 have been interpreted, the upper units are displayed in a
948 greater detail in Figs. 5, 6 and 7. A large fault is present in the centre of the profile and smaller ones
949 to the southwest. The lower part of the large fault is concealed by the chaotic expression of the
950 deposits. The small arrow in the ENE indicates the infill progradation of the depression (within the
951 black box).

952 Fig. 5: Single channel sparker seismic profile (and interpretation) perpendicular to the Gemini mud
953 volcano, displaying 4 out of 5 units. The lower boundary of Unit 2 is based on correlation with other
954 profiles. Relative current strengths are indicated by the size of the bottom current symbol and the
955 green arrow shows the increase in mounded nature of the deposits of Unit 3. The green fillings in the
956 NNE indicate when mud eruptions did not occur and sediments are deposited on top of the mud. The
957 table at the left side of the figure consists of the unit, subunit and the marine isotopic stage (MIS) in
958 which the unit is deposited.

959 Fig. 6: Single channel sparker seismic profile (and interpretation) perpendicular to the Pen Duick
960 escarpment (PDE), displaying 4 out of 5 units. The green arrow indicates the increase in mounded
961 nature of the sediments in Unit 3. The same table as for Fig. 5 is used. Relative currents strengths are
962 indicated by the size of the symbol.

963 Fig. 7: Single channel sparker seismic profile (and interpretation) perpendicular to the Pen Duick
964 escarpment, across one of the mounds at its foot (Fig. 2). The green spots within Unit 3 indicate
965 buried cold-water coral mounds (CWC) and the green dotted part in the mound on top of the
966 sediment indicates the CWC part of that mound. The yellow part of Unit 5 shows the mounded
967 sediment drift WSW of the mound. A bottom current flows along PDE and mound.

968 Fig. 8: Isopach maps of Units 2 to 5. The thicknesses are displayed in ms TWT (two-way travel time).
969 On each map, the Pen Duick escarpment and Gemini mud volcano are indicated. The uplift of the
970 PDE can be seen by the reduced thickness at its foot.

971 Fig. 9: Summarizing sketches of the contourite drift evolution along both Pen Duick escarpment (right
972 panels) and Gemini mud volcano (left panels). Relative bottom current strengths are indicated by the
973 size of the symbol. The dark orange part indicate active mud flows from the Gemini MW. The sketch
974 within Unit 5 along the PDE shows the build-up of the mounds at the foot of the PDE.

975 Fig. 10: Comparison of the evolution of the Pen Duick drift to MOW-controlled drifts in the northern
976 Gulf of Cadiz (Roque et al., 2012) and the Bay of Biscay (Van Rooij et al., 2010). Red boxes stand for
977 pre-contourite deposits, yellow for sheeted drift and green for mounded drift deposits. MIS: Marine
978 Isotopic Stage.

Figure 1
[Click here to download high resolution image](#)

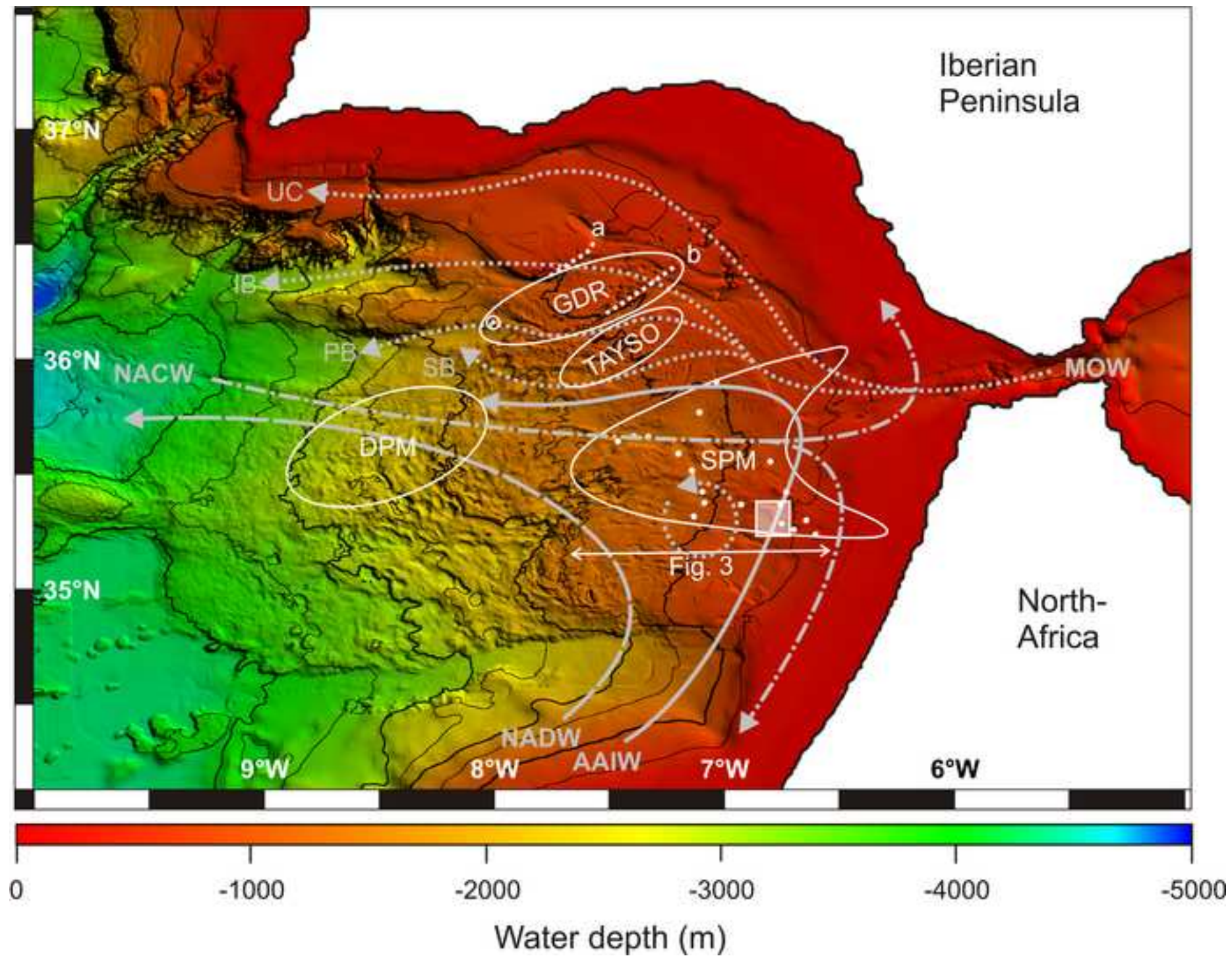


Figure 2
[Click here to download high resolution image](#)

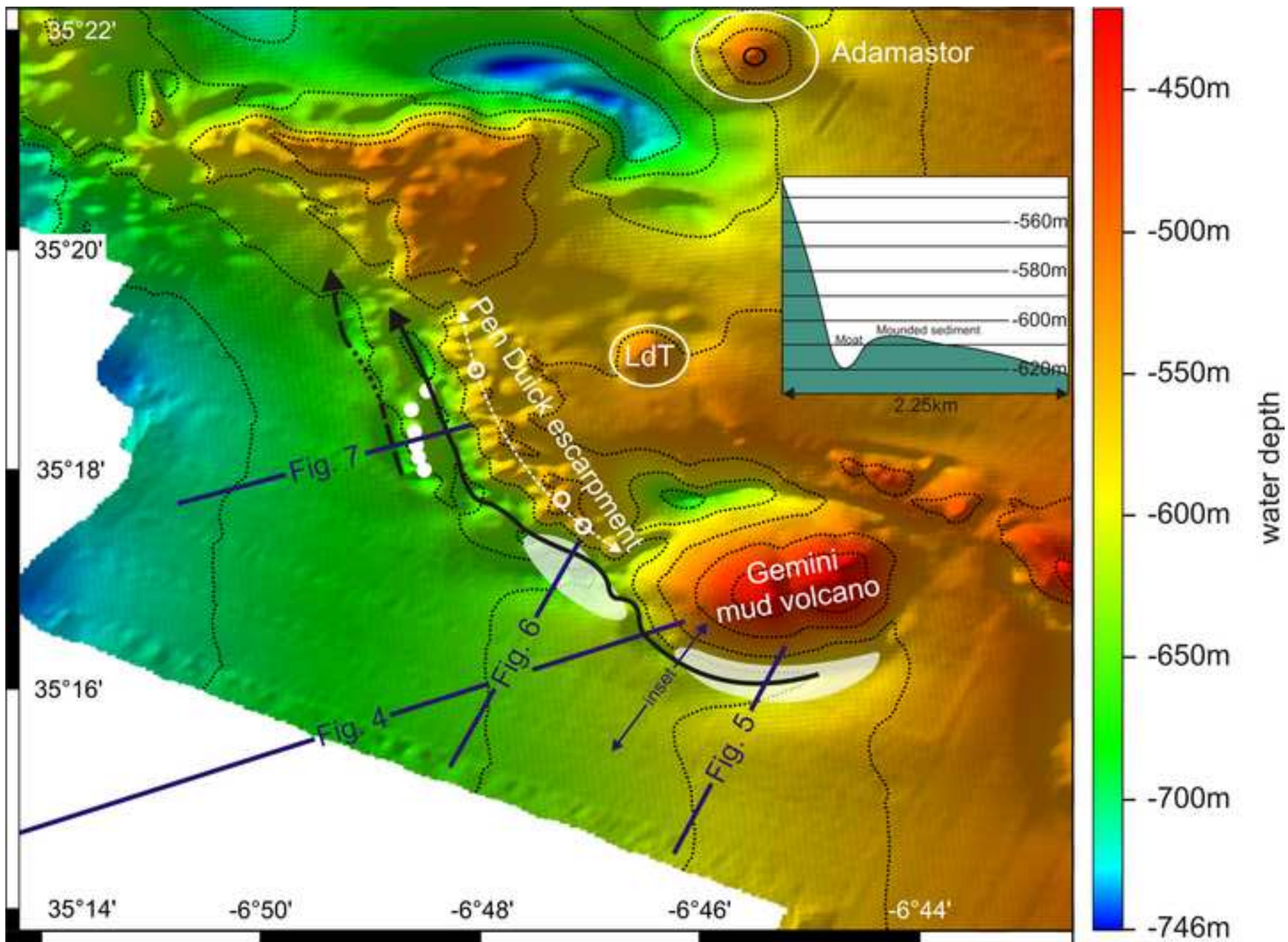


Figure 3
[Click here to download high resolution image](#)

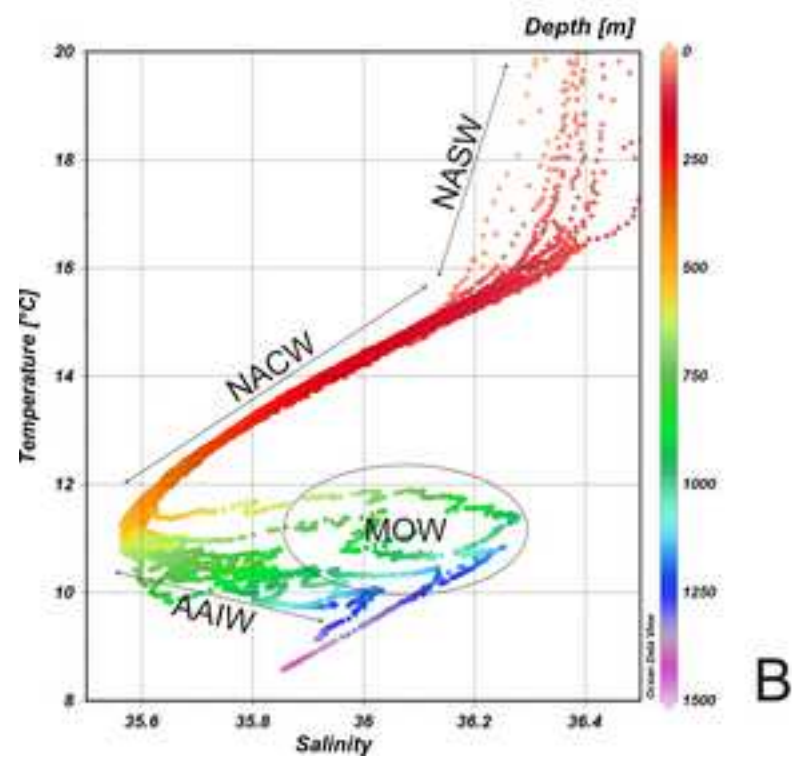
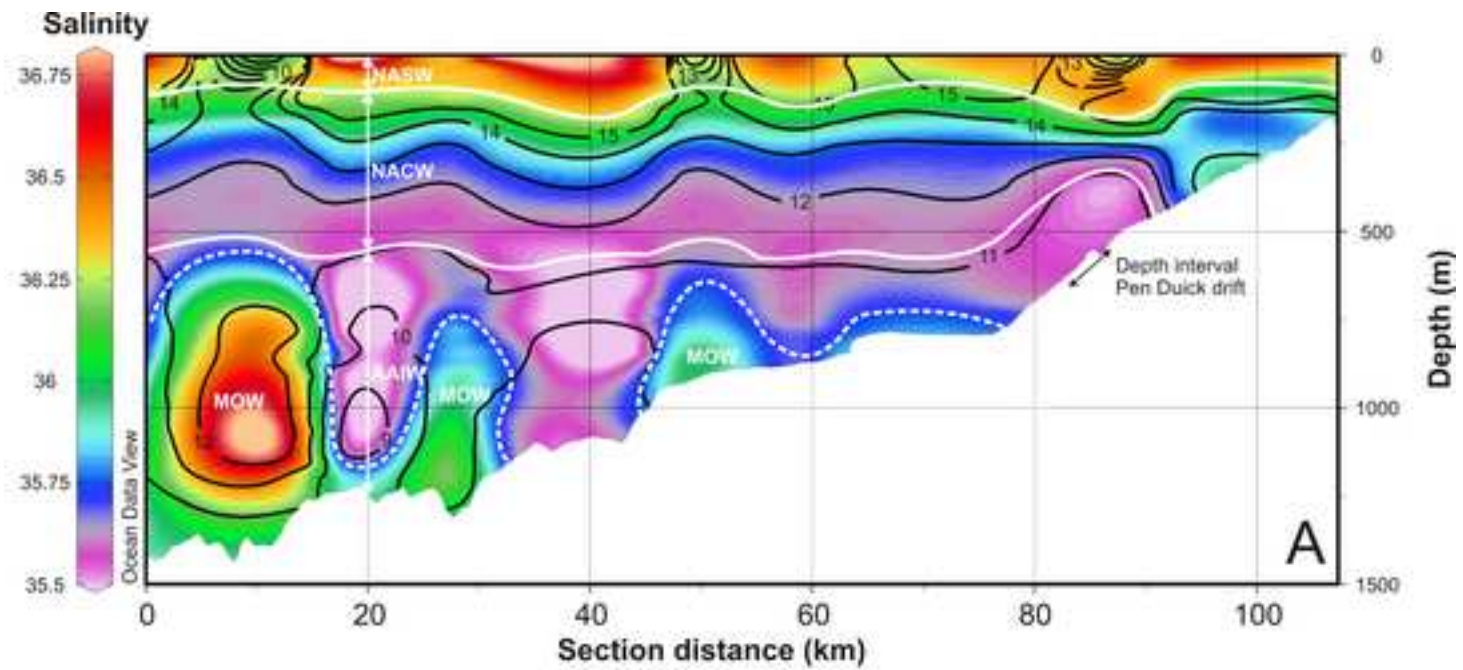


Figure 4
[Click here to download high resolution image](#)

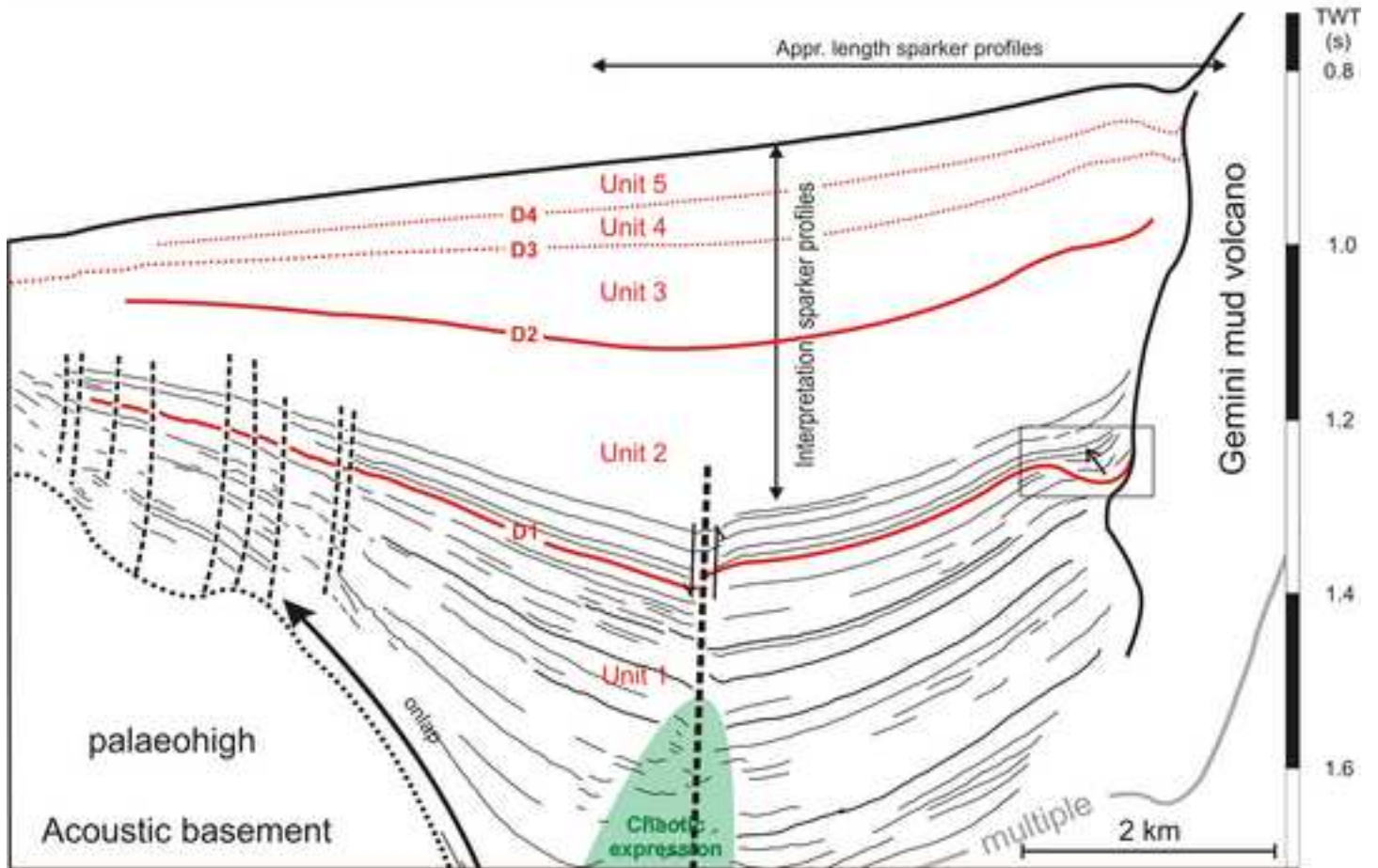
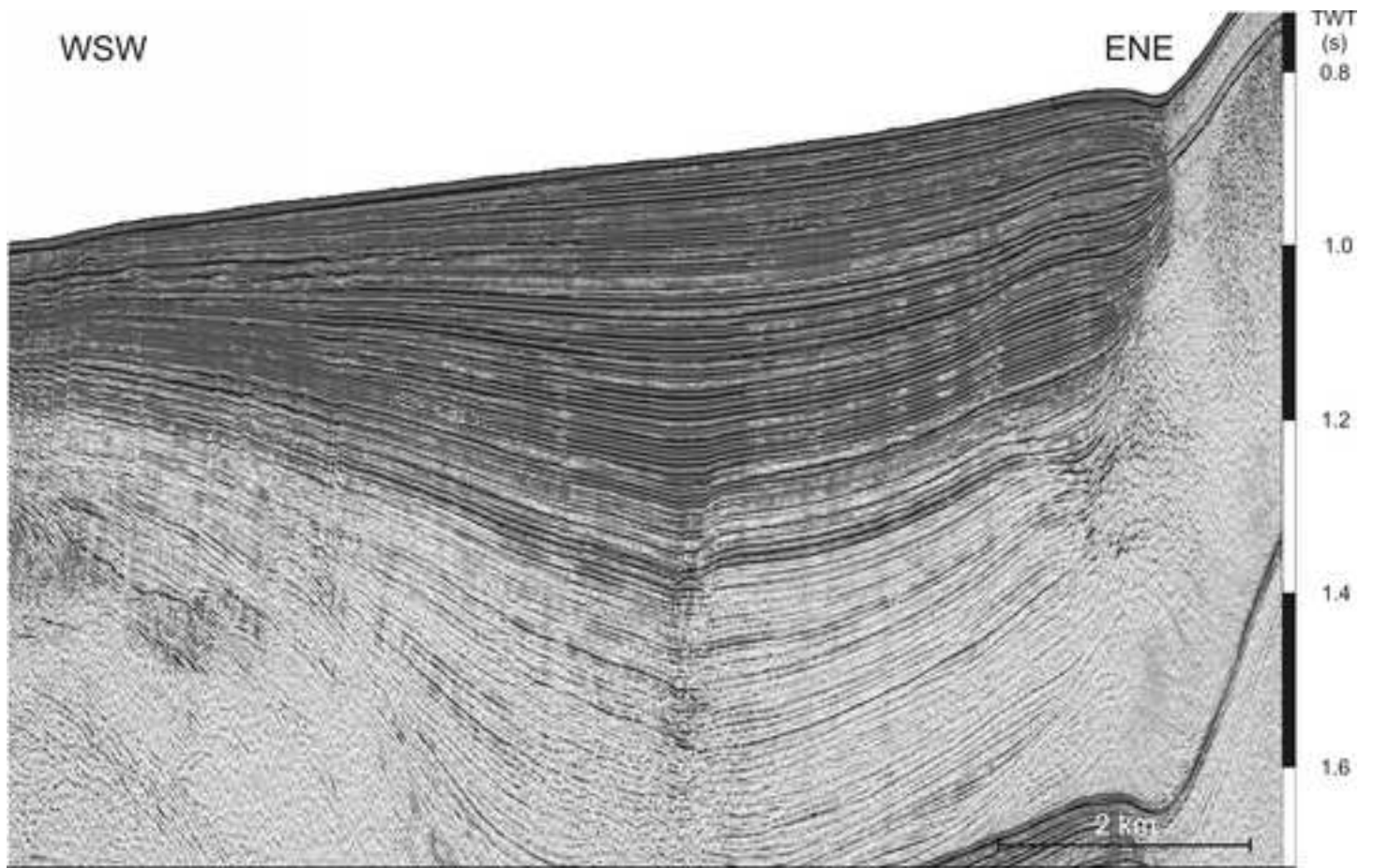


Figure 5
[Click here to download high resolution image](#)

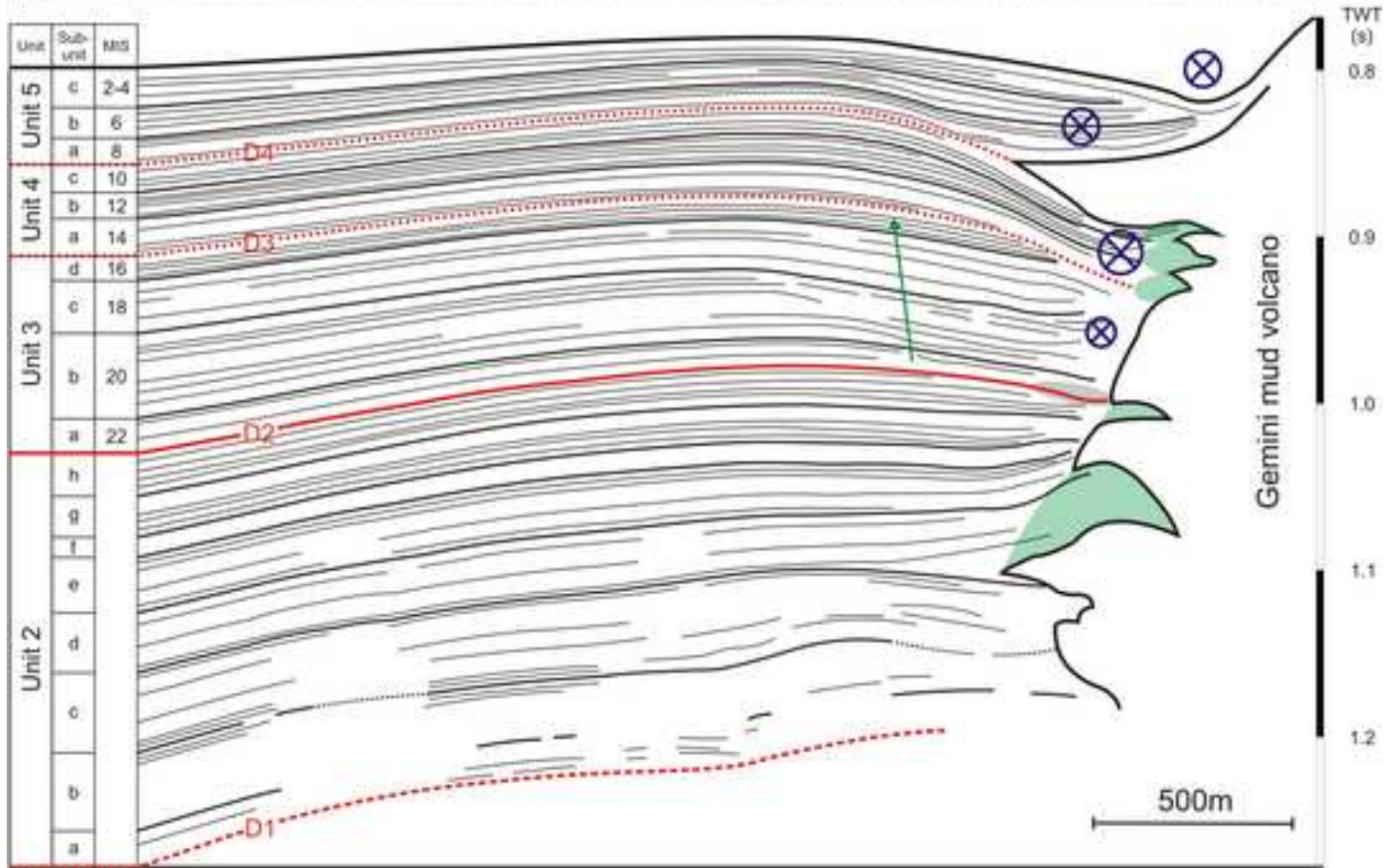
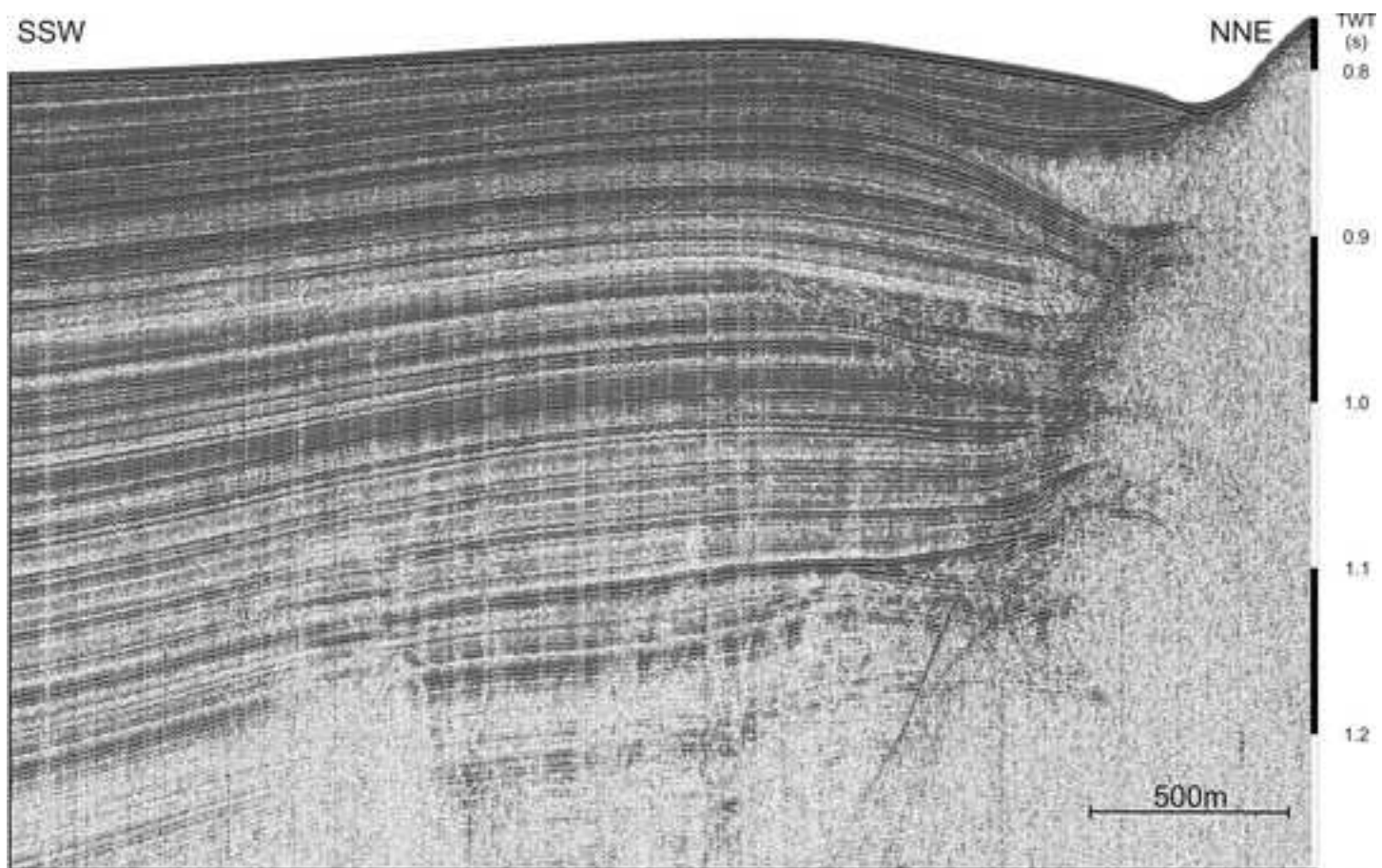


Figure 6
[Click here to download high resolution image](#)

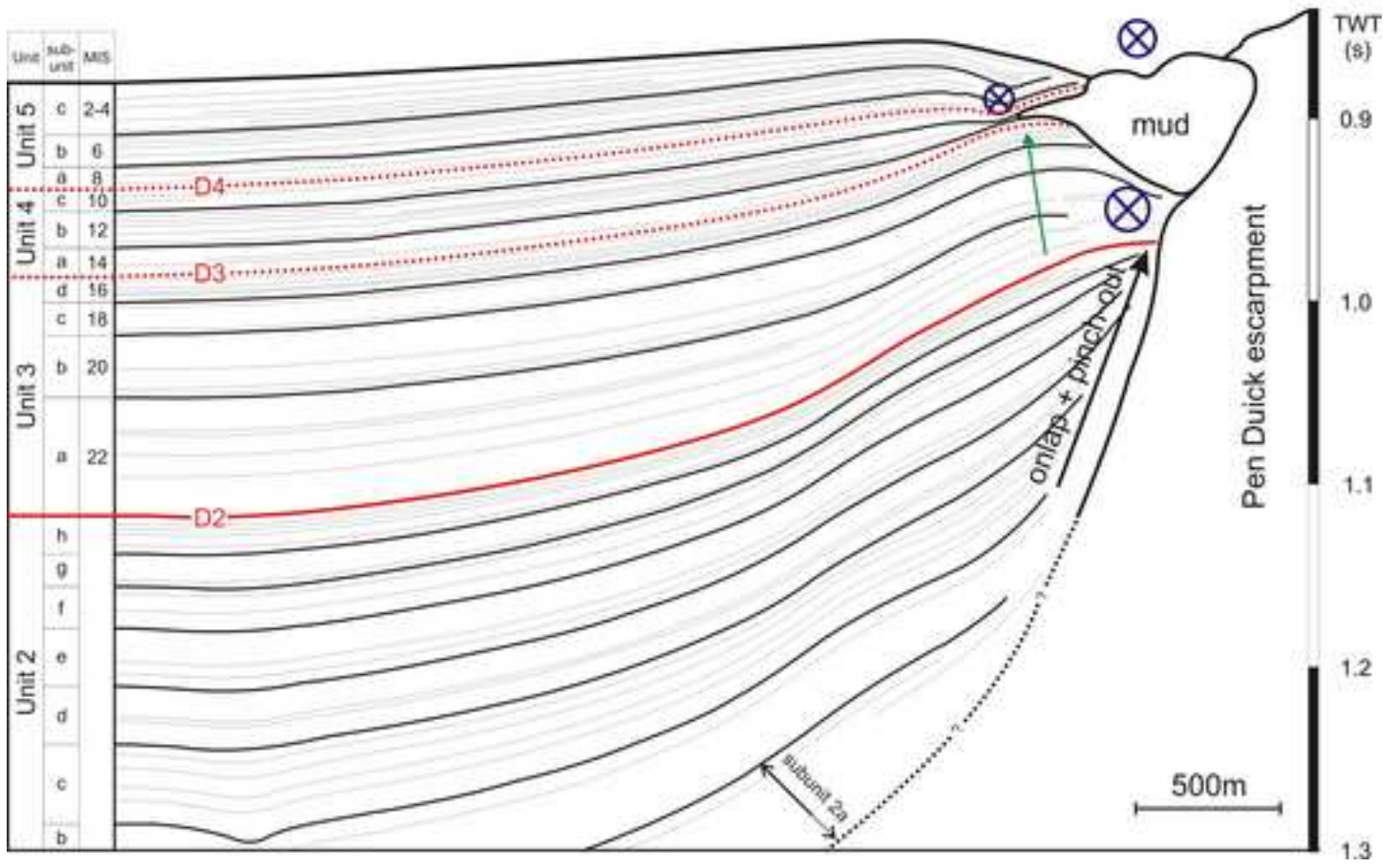
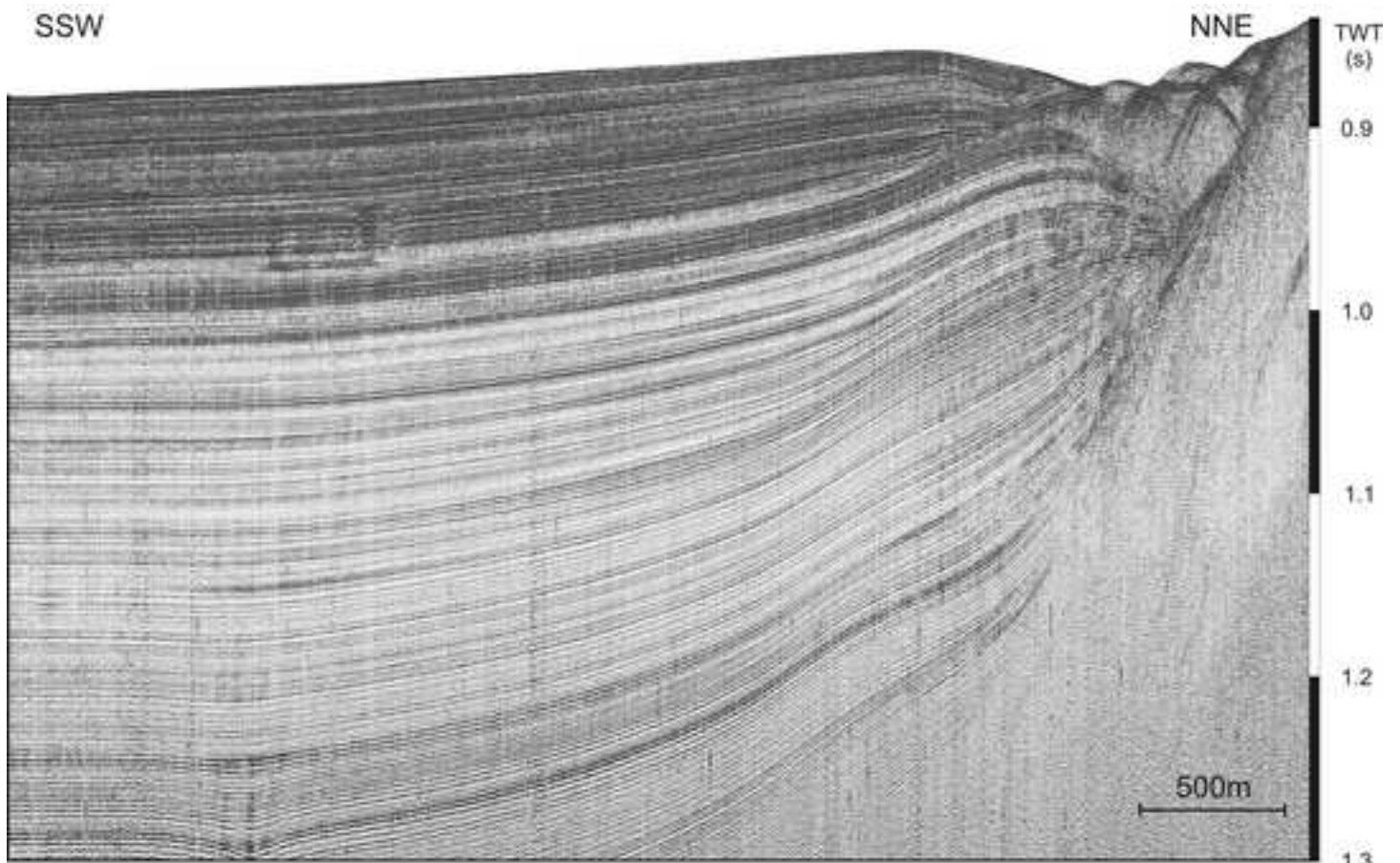


Figure 7
[Click here to download high resolution image](#)

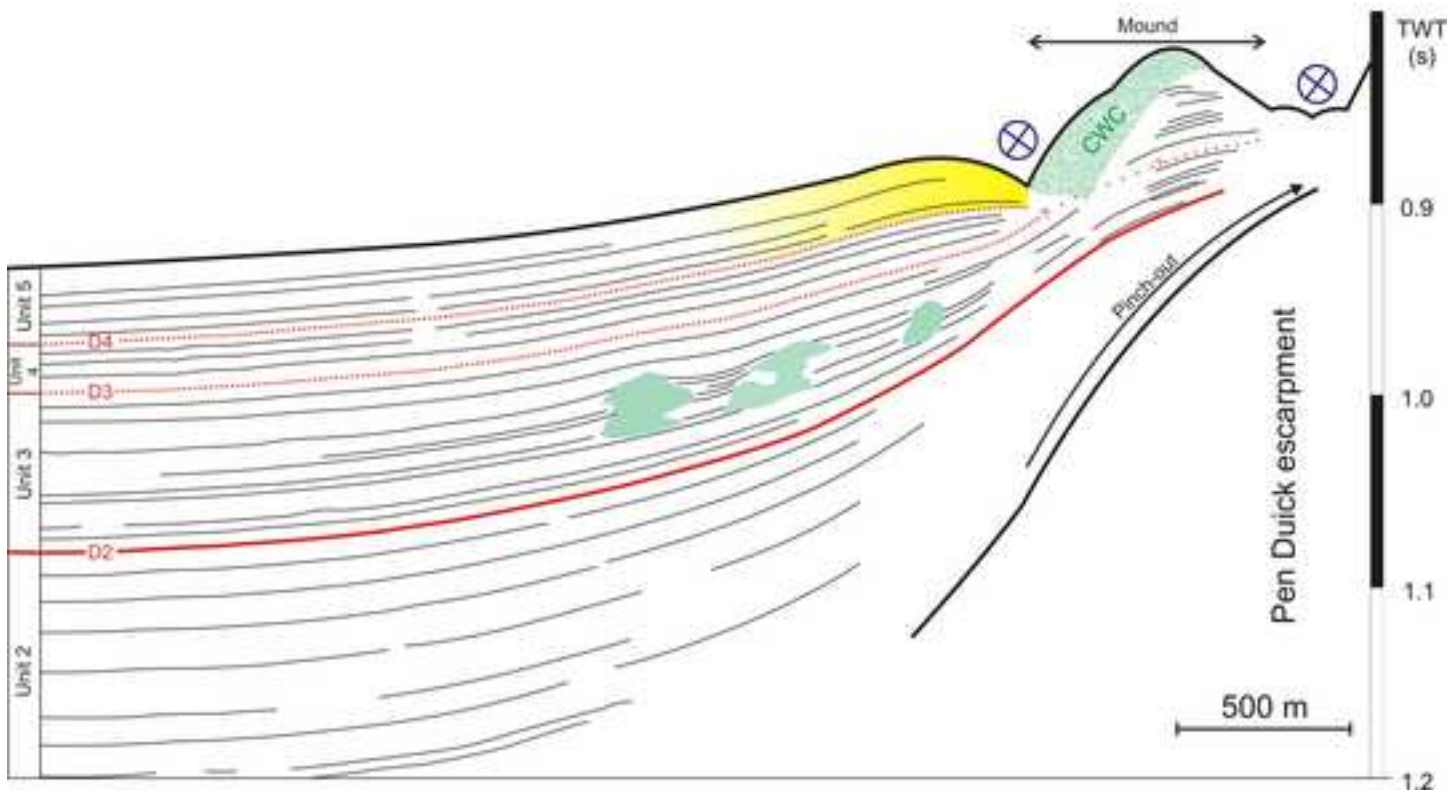
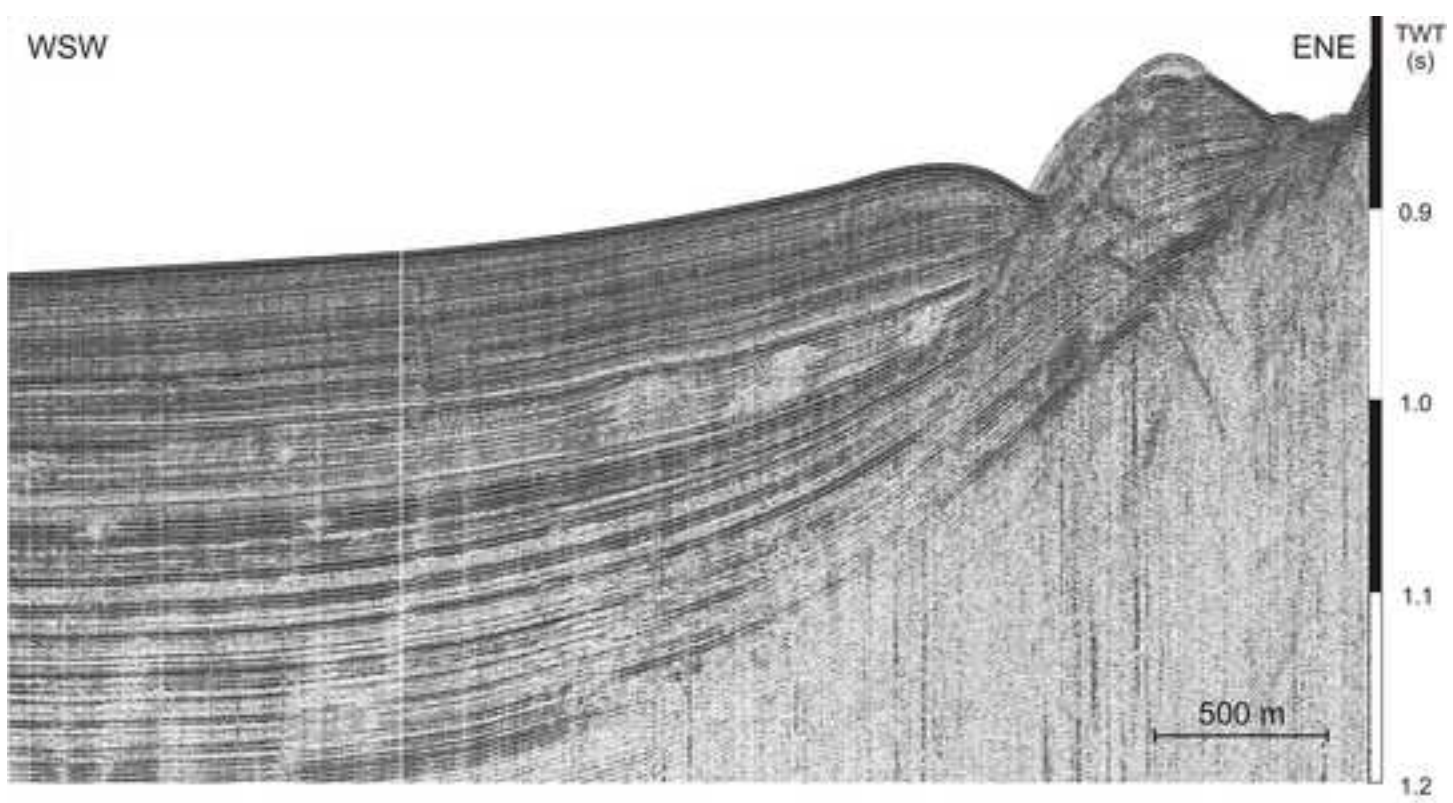


Figure 8
[Click here to download high resolution image](#)

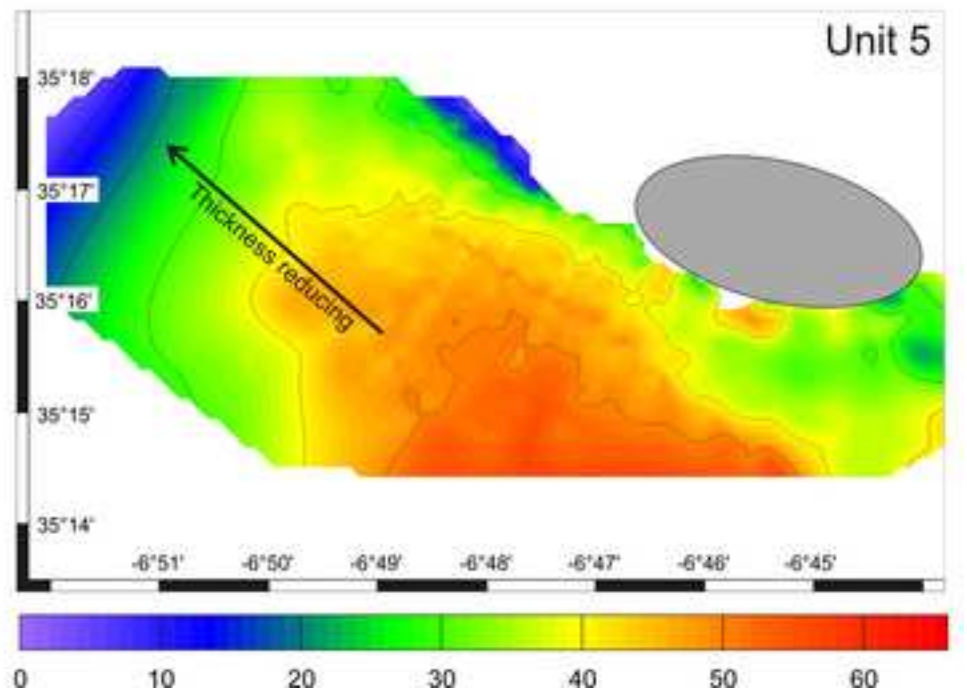
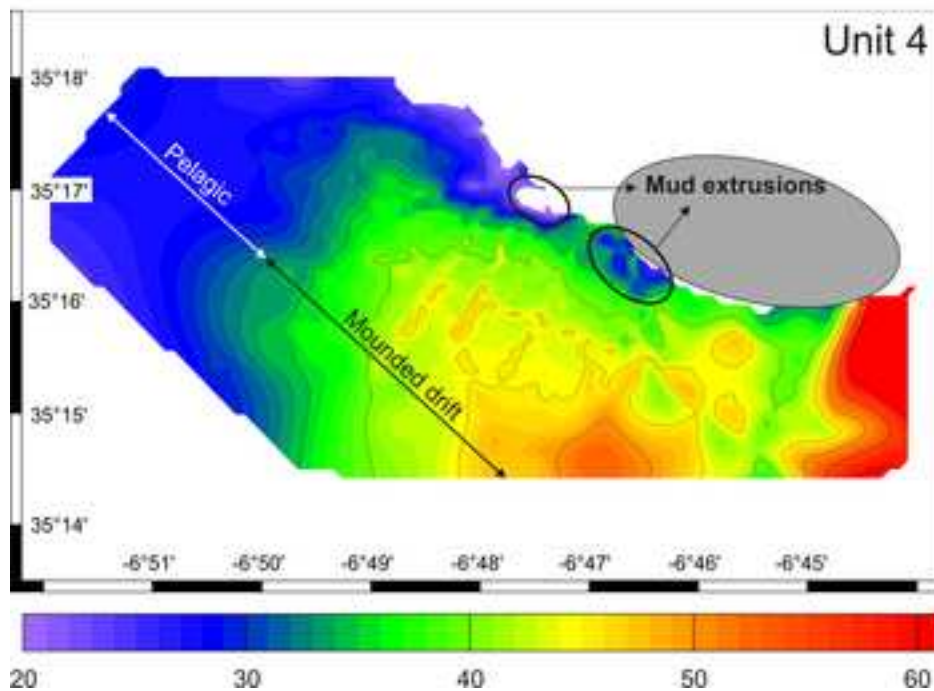
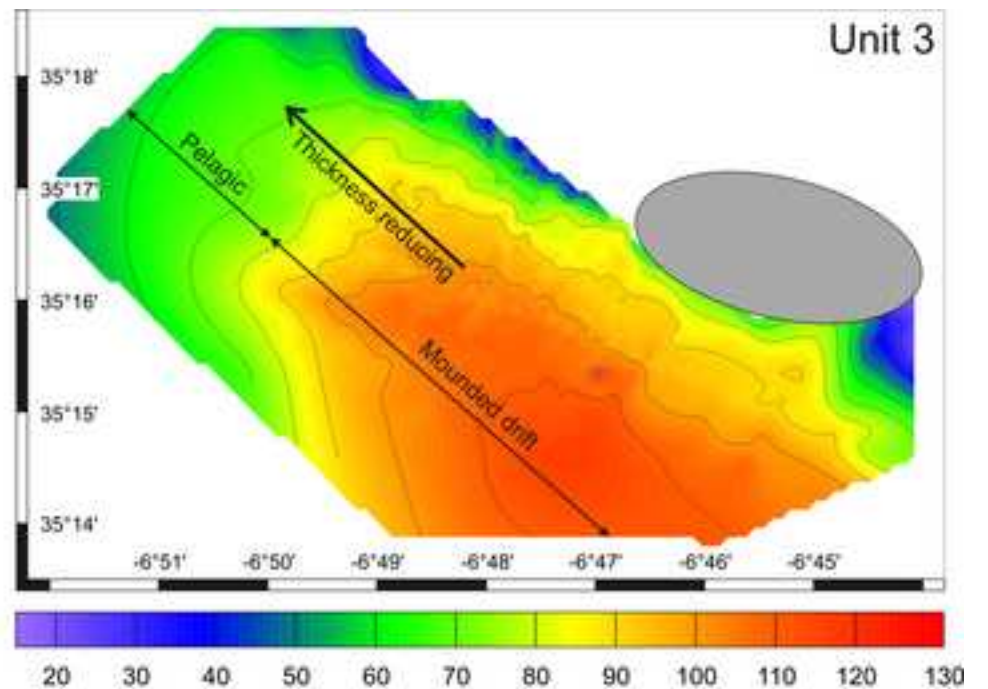
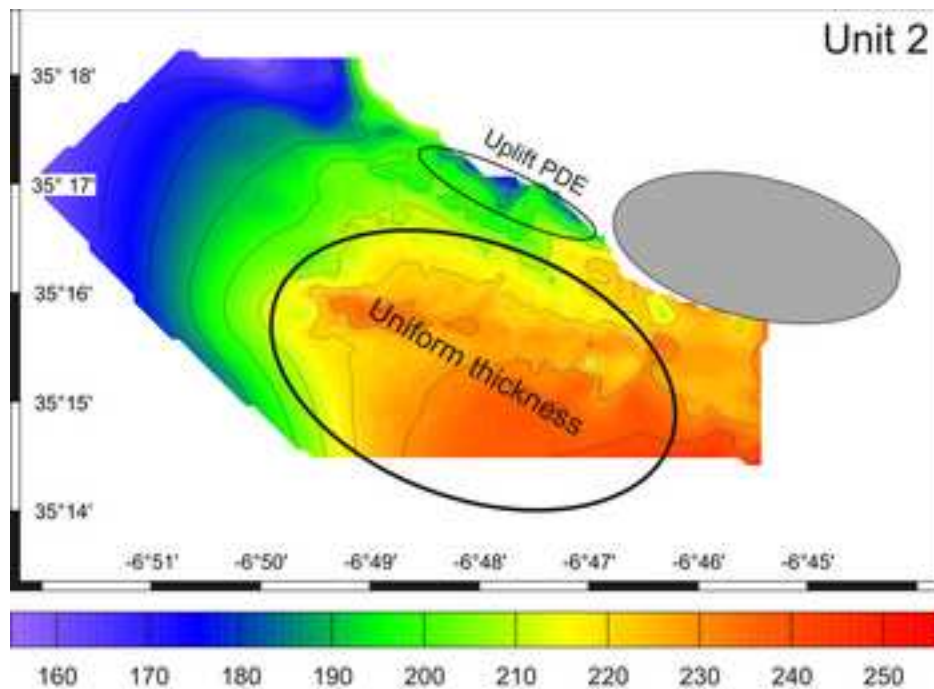
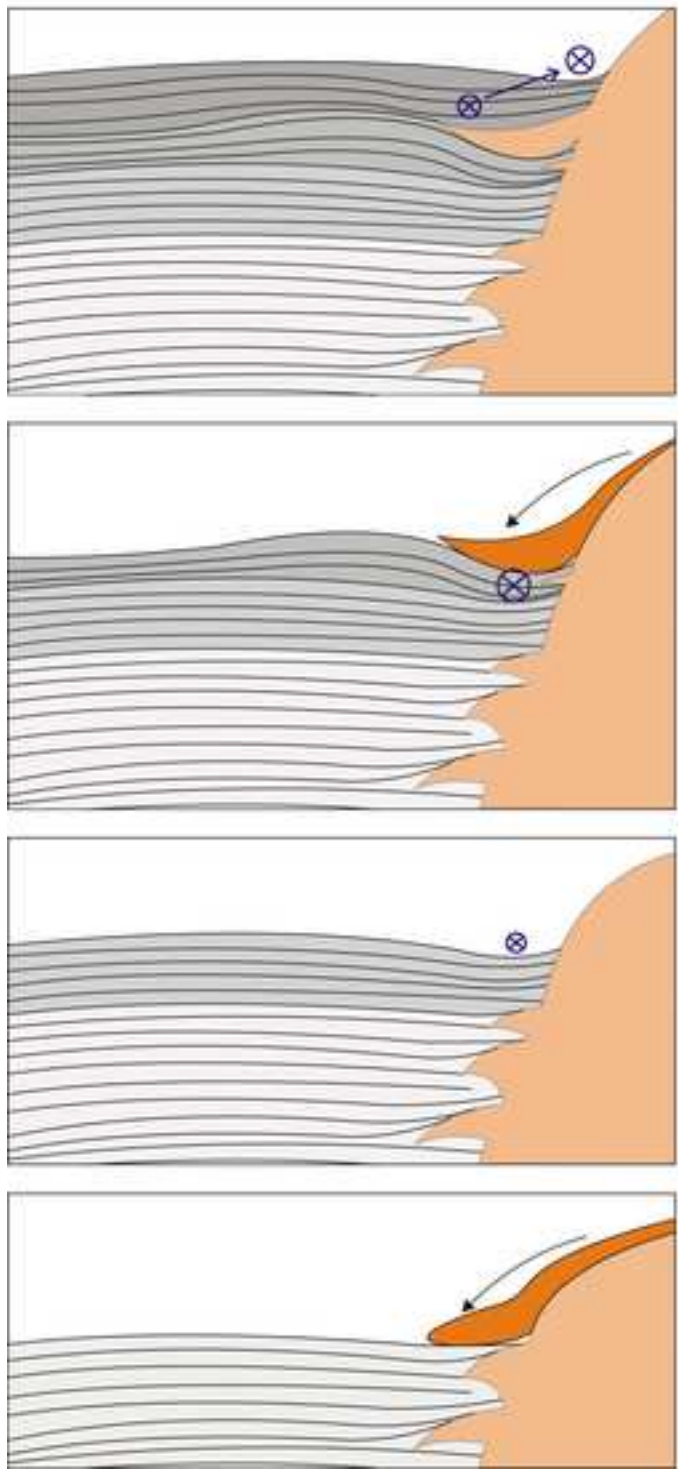


Figure 9
[Click here to download high resolution image](#)

Gemini mud volcano



Pen Duick escarpment

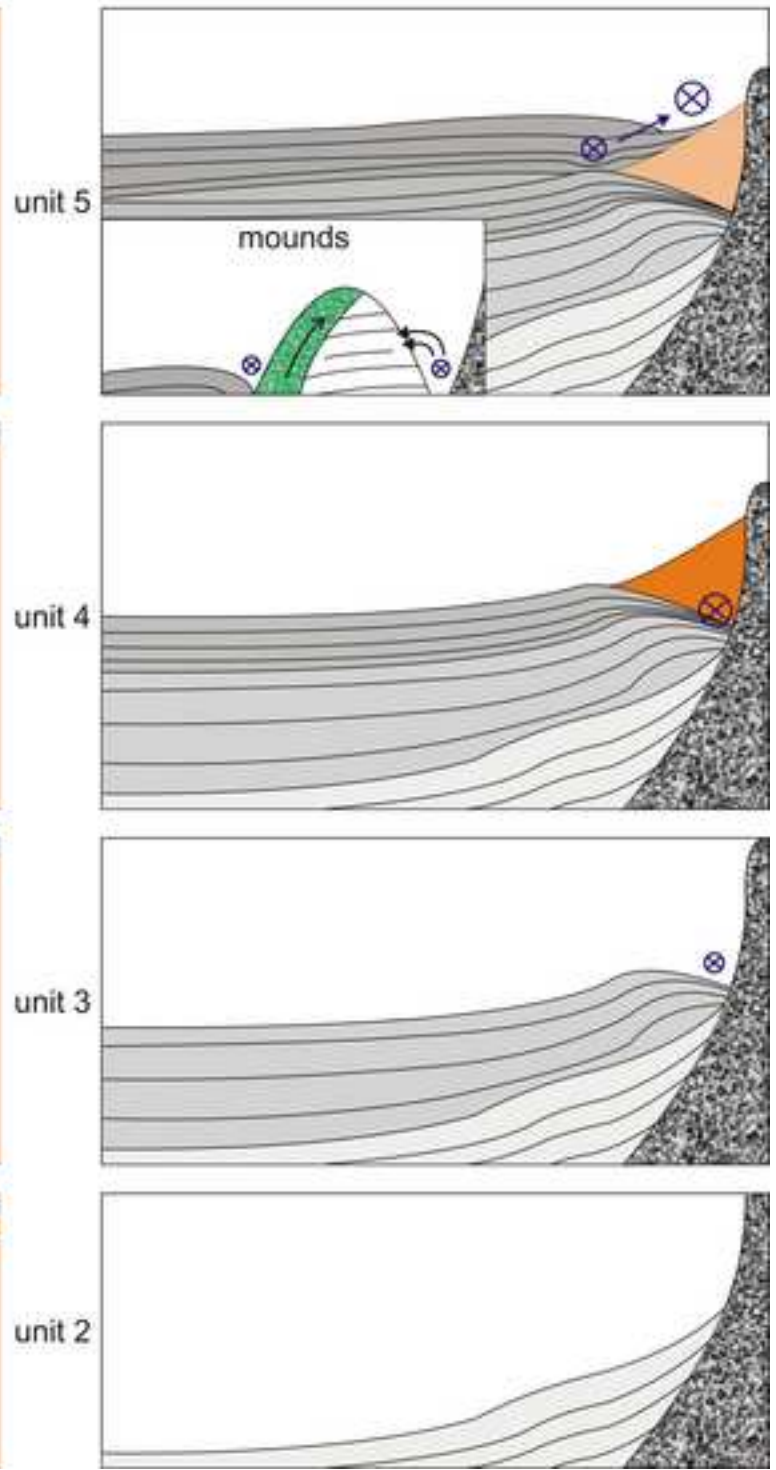


Figure 10

[Click here to download high resolution image](#)

Age		Cadiz CDS (Roque et al. 2012)	This study	Le Danois CDS (Van Rooij et al. 2010)	
Quaternary	MIS 9 MIS 12 MIS 15 MPR BQD	U5	unit 5	Unit Ua	
		-----D4-----?.....?.....?	
		H5	unit 4	Unit Ub	
		-----D3-----?.....?.....?	
		U4	unit 3	Unit Uc	
		H4	-----D2-----	-----U/M-----	
U3	unit 2	Sequence M			
Pliocene	BQD	H3	-----D1-----	-----M/L-----	
		U2	unit 1	Sequence L	
		H2			↑ ?
		U1			↓ ?
		H1			
Um					